Dispersed fluorescence spectroscopy of primary and secondary alkoxy radicals

Jin Jin, Ilias Sioutis, György Tarczay,[a] Sandhya Gopalakrishnan, Andrew Bezant, and Terry A. Miller
Laser Spectroscopy Facility, Department of Chemistry, The Ohio State University, 120 West 18th Avenue, Columbus, Ohio 43210

(Received 16 July 2004; accepted 17 September 2004)

Dispersed fluorescence (DF) spectra of 1-propoxy, 1-butoxy, 2-propoxy, and 2-butoxy radicals have been observed under supersonic jet cooling conditions by pumping different vibronic bands of the $\tilde{B}$-$\tilde{X}$ laser induced fluorescence excitation spectrum. The DF spectra were recorded for both conformers of 1-propoxy, three conformers of the possible five of 1-butoxy, the one possible conformer of 2-propoxy, and two conformers of the possible three of 2-butoxy. Analysis of the spectra yields the energy separations of the vibrationless levels of the ground $\tilde{X}$ and low-lying $\tilde{A}$ electronic state as well as their vibrational frequencies. In all cases, the vibrational structure of the DF spectra is dominated by a CO stretch progression yielding the ν_{CO} stretching frequency for the $\tilde{X}$ state and in most cases for the $\tilde{A}$ state. In addition to the experimental work, quantum chemical calculations were carried out to aid the assignment of the vibrational levels of the $\tilde{X}$ state and for some conformers the $\tilde{A}$ state as well. Geometry optimizations of the different conformers of the isomers were performed and their energy differences in the ground states were determined. The results of the calculation of the energy separations of the close-lying $\tilde{X}$ and $\tilde{A}$ states of the different conformations are provided for comparison with the experimental observations. © *2004 American Institute of Physics.* [DOI: 10.1063/1.1814104]

I. INTRODUCTION

The oxidation of hydrocarbons is among the most important of chemical processes, with combustion and the degradation of volatile organic compounds injected in our atmosphere being the prime examples. The reactions of the simplest oxygen-containing organic radicals, e.g., alkoxy, RO, and peroxy, RO_2 radicals, affect the yield of ozone, air toxics, and organic aerosols in the atmosphere.[1] Combustion of hydrocarbon fuels at temperatures $\leqslant$1000 K share many mechanistic details with their atmospheric oxidation. The existence of multiple reaction pathways for these radicals complicates efforts for the understanding of the potential oxidation scheme of hydrocarbons, as it is the competition among the various radical reactions pathways that determines the end products of the oxidation.[2] Hence elucidation of their chemistry is paramount for obtaining a better understanding of combustion processes and the impact of hydrocarbons in the atmosphere.

This paper concerns itself with the alkoxy radicals. There have been extensive spectroscopic investigations, via the $\tilde{B}$-$\tilde{X}$ electronic transition, of the smaller alkoxy radicals[3] as well as some studies of larger ones.[4] Laser-induced fluorescence (LIF) excitation spectroscopy of jet-cooled radicals has provided a good deal of information about the excited states. Very recently, high-resolution rotationally resolved spectroscopy of a number of bands of jet-cooled primary alkoxy radicals[5,6] yielded detailed information about the structure and geometries of both the $\tilde{B}$ and $\tilde{X}$ states. It was found that various bands of the LIF spectra uniquely correlated with different conformers of a given structural isomer.

However, information about the excitation energy of the low-lying $\tilde{A}$ state as well as the ground $\tilde{X}$ state's vibrational structure and dynamics has been relatively sparse. A suitable technique for investigating this area is laser excited, dispersed fluorescence (DF) spectroscopy. It has been used to probe the vibronic levels in the ground state of CH_3O[7] and C_2H_5O.[8] However, DF studies have not been extended to larger alkoxy radicals thus far.

The alkoxy radicals can be viewed as derivatives of methoxy. While the nominal point-group symmetry of methoxy is C_{3v}, for all other alkoxy radicals the symmetry is lower (except possibly for *t*-butoxy). Upon the lowering of the point-group symmetry, the ground electronic state of methoxy ^2E is resolved into a pair of states with the ground state designated as $\tilde{X}$ and the lowest lying excited state as $\tilde{A}$. The first excited state of methoxy is electronically nondegenerate and corresponds to a state designated as $\tilde{B}$ for the alkoxies larger than methoxy (except *t*-butoxy). The LIF excitation spectrum involves the $\tilde{B}\leftarrow\tilde{X}$ transition while the DF spectra involve the $\tilde{B}\rightarrow\tilde{A}$ and $\tilde{B}\rightarrow\tilde{X}$ emission. The $\tilde{B}$ state excitation is well known to be nominally a one-electron excitation of a p-σ bonding electron to fill the half-filled p-π orbital localized on the O atom.

In the present work, LIF spectroscopy was combined with supersonic free jet expansion techniques to record the

[a]Permanent address: Department of General and Inorganic Chemistry, Eötvös University, P. O. Box 32, H-1518 Budapest 112, Hungary.

TABLE I. Summary of the conditions used for the experiments with the primary and secondary alkoxies.

Alkoxies	Primary	Secondary
Temperature of the sample bomb (°C)	−5	10
Backing pressure (psi)	90	40,80[a]
Slit width (μm)	60	150[b]
Resolution (cm^{-1})	15	30–35
Accumulation time (min)	40	60[c]
Grating (grooves/mm)	1800	1800

[a]The backing pressure in the 2-propoxy experiment was kept at 40 psi and for 2-butoxy at 80 psi.
[b]The DF emission following the LIF excitation of the first member of the CO stretch progression of 2-propoxy was collected with an entrance slit width of 50 μm.
[c]For 2-butoxy the accumulation time for the DF collection via bands A through D was extended at least 3 h for the first 2000 cm^{-1} redshifted from the pumping frequency.

DF spectra from a number of $\tilde{B}$ state levels of the 1- and 2-isomers of the propoxy and butoxy radicals. These spectra can yield the direct measurements of the $\tilde{A}$-$\tilde{X}$ electronic state separation. Emission was observed primarily to the CO vibrationless level and excited stretch and CCO vibrational modes (or modes coupled with these motions) of both the $\tilde{X}$ and $\tilde{A}$ states. The DF data also serve to support the identification of multiple conformations of the alkoxy radicals.

Extensive quantum chemical computations were carried out as an aid to the assignment of the observed vibronic bands. Both the $\tilde{A}$-$\tilde{X}$ energy gap and the $\tilde{X}$ and $\tilde{A}$ vibrational frequencies can be used as benchmarks against which theoretical treatments of these complex radicals can be measured. Information about the $\tilde{A}$-$\tilde{X}$ energy separation is important for a better understanding of the vibronic interactions between these close-lying, lowest energy states. The $\tilde{A}$-$\tilde{X}$ separation is also very important for understanding the kinetics and detailed dynamics of the alkoxy radicals as the degree of $\tilde{A}$ state participation in thermal reactions is dependent upon its excitation energy. The separation is also critical to an understanding of the ground state spin-rotation splittings.

The remainder of this paper is organized as follows. In Sec. II an outline of the experimental details is given. The analysis of the experimental spectra takes place in Sec. III. Section IV centers on a number of aspects pertaining to the structure and spectra of the primary and secondary alkoxies. The paper's conclusions are presented in Sec. V.

II. EXPERIMENTAL DETAILS

The alkyl nitrite precursor molecules were prepared by the dropwise addition of the concentrated sulfuric acid to a saturated solution of $NaNO_2$ and the corresponding alcohol.[9] A few torr of the alkyl nitrite vapor was entrained into the jet flow by passing helium at a suitable backing pressure over the liquid contained in a stainless steel reservoir maintained at a suitable temperature depending upon the vapor pressure. A summary of the experimental conditions is given in Table I. The seeded flow was then expanded through a 300 μm standard pulsed nozzle (general valve) into the jet chamber which was evacuated by a mechanical booster pump backed by a rotary oil pump. To produce the alkoxy radicals, photolysis of the precursors just above the throat of the nozzle was performed using the output of a tripled Nd:yttrium aluminum garnet (YAG) laser (Quanta-Ray DCR-2, 355 nm). This produced the desired alkoxy radicals which were then probed about 10 mm downstream from the photolysis laser. The probe beam was the frequency doubled output (Inrad Autotracker II) of a tunable dye laser (SpectraPhysics PDL-3) pumped by the second harmonic of a Nd:YAG (Quanta-Ray DCR) laser at 532 nm. This work required the use of three laser dyes (LDS 698, 750, and 751) which spanned appropriate spectral regions for the DF excitation frequencies. The delay time between the firing of the photolysis and dye lasers, along with the time delay and the opening time of the nozzle, were controlled by a pulse generator (Stanford Research DG535).

The photolysis and probe beams counterpropagated through the vacuum chamber. The fluorescence signal was collected perpendicularly to the laser beams. On one side of the chamber, the fluorescence emission was collimated by an 1 in. diameter lens ($f/1$) and a second lens focused the radiation onto the photocathode of the photomultiplier tube (EMI 9659Q) connected to an amplifier. The amplified LIF signal was integrated by a boxcar averager, digitized by an A/D converter and fed into a personal computer for further data processing. On the other side of the chamber, the fluorescence emission was dispersed by a Spectra Pro 300i monochromator using a 1800 grooves/mm grating and then imaged onto an intensified charge-coupled device. The detection of the dispersed photons for the secondary alkoxies was done exclusively with the Princeton Instruments PI-MAX512HB camera. In the case of the primary alkoxies two cameras were used, the above one and a second one, Princeton Instruments PI-MAX512RB. The emission frequencies reported for the DF spectra of the alkoxies were obtained by calibrating them against a Fe-Ne lamp, or known laser frequencies.

III. RESULTS

DF spectra were observed for both the propoxy and butoxy radicals. There are two isomers for propoxy; the linear chain isomer 1-propoxy and the branched chain one denoted as 2-propoxy, often referred to as isopropoxy. In the case of the butoxy radicals, there exist four possible isomers two of which will be the focus of this work, namely, the 1-butoxy and 2-butoxy species.

It is known that different conformations can exist for a given structural isomer. Therefore, theoretically speaking, one should anticipate two different conformers for 1-propoxy and one possible conformation for isopropoxy. Five conformations are possible for 1-butoxy and three for 2-butoxy. High-resolution spectroscopic studies have identified,[5,6] via detailed analysis of the rotational structure of the vibronic bands, both conformers of 1-propoxy and three of 1-butoxy populated in the free jet expansion. The conformers for 1-propoxy are denoted as *gauche* G and *trans* T. G is a C_1-symmetry structure and T is of C_s symmetry. For 1-butoxy the corresponding conformations (point-group symmetries) are G_1T_2 (C_1), T_1T_2 (C_s), and T_1G_2 (C_1).

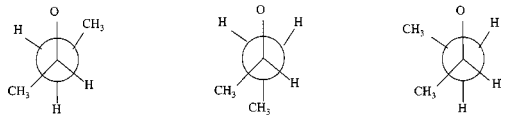

FIG. 1. Newman projections of three unique conformational structures of 2-butoxy at their local minima. The designation of the conformers is based on the value of the dihedral angle ϕ which is formed by C_2-C_1-O and $C_1-C_2-C_3$ planes; rotation about the C_1-C_2 bond changes ϕ from 60° (*gauche clockwise* $G+$), to 180° (*trans* T) and $-60°$ (*gauche counterclockwise* $G-$).

The reflection plane of symmetry in 2-propoxy classifies it as a C_s-symmetry structure. 2-Butoxy possesses the *gauche clockwise* conformer $G+$ (C_1), the *trans* T (C_1) conformer, and the *gauche counterclockwise* conformation $G-$ (C_1) (see Fig. 1). Because of the chiral stereocenter in 2-butoxy, enantiomers are expected in each conformer. They should give identical spectra, thus there are only three unique conformer spectra possible for 2-butoxy.

A. Quantum chemistry calculations

To aid the assignment process we have carried out a number of quantum chemistry calculations. These included (i) the geometry optimization of the different conformers of the primary and secondary radicals and the determination of their relative energy difference in their ground electronic state; (ii) the calculation of the energy separations of the close-lying $\tilde{A}$ and $\tilde{X}$ states for each conformer; (iii) the calculation of the harmonic vibrational frequencies of the conformers in their ground state. These calculations have been performed by the GAUSSIAN 98 program package[10] at the B3LYP/6-31+G* level of theory. The geometry optimization of all of the conformers was done at C_1 symmetry. Tables II, III, and IV–VII summarize the computational results (i), (ii) and, in part (iii), respectively. Table III also includes some results (obtained by the ACESII program package[11]) for selected alkoxy radicals performed at the equation-of-motion excitation energy coupled cluster singles and doubles (EOM-EE-UCCSD)[12] level of theory using the cc-pVDZ basis set. Tables IV–VII refer to only one conformation of each structural isomer, while Tables I–XII of the Supplementary Material[13] contain a complete summary of the calculated harmonic vibrational frequencies for all of the experimentally observed conformations in their ground electronic state. (In the case of 2-butoxy, the vibrational frequencies of all three of the conformers are reported, although only two conformations are identifiable in the DF spectra.) The calculations of the $\tilde{A}$ state vibrational frequencies for the C_s conformers are also summarized in the Supplementary Material. Tables IV–VII include all frequencies lower than $\approx 1500\ \mathrm{cm}^{-1}$ labeled following the Mülliken notation scheme[14] for a C_1 molecule. These lower frequency vibrations are the ones relevant to the interpretation of the DF spectra; the remaining higher vibrational frequencies are, as noted, given in the Supplementary Material.

The first two columns of the tables label and give the value of the harmonic frequencies obtained at the C_1-symmetry minimum while their vibrational character is described in terms of (i) CO stretch and (ii) CCO deformation, and (iii) other motions in the remaining three columns. These determinations are based upon visual inspections of the vibrational motion as displayed by GAUSSVIEW (Gaussian, Inc.). It is a useful guide for the assignment process to approximately know the degree of participation of the CO stretch and the CCO deformation in the vibrational character of each mode, since for these directions alone are there substantial differences in the $\tilde{X}$ and $\tilde{B}$ geometry leading to sig-

TABLE II. Energy differences (in cm^{-1}) relative to the energy of the lowest energy conformation of the primary and secondary radicals in their ground electronic state as obtained at the B3LYP/6-31+G* level of theory.

Alkoxy	Conformer	E[a]
1-propoxy	G	0
	T	20
1-butoxy	G_1T_2	0
	T_1T_2	62
	T_1G_2	339
2-propoxy		0
2-butoxy	$G+$	0
	T	254
	$G-$	314

[a]No zero-point energy correction was applied. For all of the alkoxy radicals, the geometry optimization led to distinct unique conformations and was done at the C_1-symmetry.

TABLE III. Experimental and calculated $\tilde{A}$-$\tilde{X}$ energy separation (in cm^{-1}) of a number of open-chain alkoxy radicals.

	Past and present studies	
Alkoxies[a]	Calculated[b]	Experimental
Ethoxy ($^2A'$)	314[380]	364,[c] 355(10)[d]
1-propoxy, T ($^2A''$)	225[369]	321(10)[e]
1-propoxy, G (^2A)	[8]	214(10)[e,f]
2-propoxy ($^2A'$)	101	68(10),[e,f] 1225(65)[d,f]
1-butoxy, T_1G_2 (^2A)	⋯	271(10)[e]
1-butoxy, T_1T_2 ($^2A''$)	169	292(10)[e]
1-butoxy, G_1T_2 (^2A)	⋯	129(10)[e,f]
2-butoxy, "B" (^2A)	⋯	55(10)[e,g]
2-Butoxy, "A" (^2A)	⋯	125(10)[e,g]

[a]The symmetries of the computed ground electronic states of the alkoxy radicals are included in parenthesis. The primed symmetry labels refer to the nominal C_s point group whereas the unprimed are under C_1 symmetry.
[b]The adiabatic $\tilde{A}$-$\tilde{X}$ energy separations were calculated at the B3LYP/6-31+G* level of theory, except for those included in brackets which were done at the EOM-EE-CCSD/cc-pVDZ level of theory. The energy separation is calculated as the difference between the C_1 energy minimum of the $\tilde{X}$ state and the C_s energy minimum of the $\tilde{A}$ state.
[c]See Ref. 8. We have reassigned the transition previously assigned to ν_{18} to the vibrationless level of the $\tilde{A}$ state. The average value of the frequency was recalculated using the raw data in Table 2 of the reference.
[d]See Ref. 19.
[e]The $\tilde{A}$-$\tilde{X}$ separation obtained from the present DF experiments.
[f]See text for possible caveats.
[g]Average of two values, see text for details.

TABLE IV. The calculated lowest 17 vibrational frequencies (in cm^{-1}) of the T conformer of 1-propoxy radical in its ground electronic state as obtained at the B3LYP/6-31+G* level of theory.

Assignment	$\tilde{X},T$ B3LYP[a]	CO stretch	CCO deformation[b]	Q[c]
ν_{11}	1436(a')	Small		CH_3, CH_2 rock, CC stretch
ν_{12}	1414(a')	Medium		CH_2 rock, CC stretch
ν_{13}	1377(a')		Small	CH_3, CH_2 rock
ν_{14}	1328(a')	Small		CH_3, CH_2 rock
ν_{15}	1305(a'')			CH_3, CH_2 rock
ν_{16}	1238(a'')			CH_3, CH_2 rock, CH_2 torsion
ν_{17}	1128(a')		Medium	CH_3, CH_2 rock, CC stretch, CCC motion
ν_{18}	1074(a')	Large		CH_3, CH_2 rock, CC stretch
ν_{19}	1034(a')	Medium		CC stretch
ν_{20}	967(a'')			CH_3, CH_2 rock
ν_{21}	889(a')		Medium	CH_3, CH_2 rock, CC stretch
ν_{22}	771(a'')			CH_3, CH_2 rock, CH_2 torsion
ν_{23}	475(a')		Large	CCC bend
ν_{24}	307(a'')			CH_2 torsion
ν_{25}	270(a')		Medium	CCC bend
ν_{26}	230(a'')			CH_3, CH_2 torsion
ν_{27}	119(a'')			Backbone flex

[a]The unscaled harmonic frequencies were obtained at the C_1-symmetry minimum and their symmetries under the C_s point group are included in parenthesis. The labeling of the vibrational modes follows the Mülliken notation scheme (Ref. 14) assuming C_1 symmetry.

[b]For a' symmetry modes the CCO deformation is an in-plane bend and for a'' symmetry modes it is an out-of-plane twist.

[c]The contributions of various internal coordinates Q to the normal mode indicated in the first column are listed, other than the CO stretch or CCO deformation which are listed in the preceding two columns with a qualitative indication of their magnitude.

nificant Franck-Condon factors for progressions in modes containing these motions. The tables contained in the Supplementary Material show that generally there appear to be few pronounced differences among the vibrational frequencies of the possible conformers for the alkoxy radicals.

Table II gives the calculated energies of the conformers. It is worthwhile noting that the conformer that is calculated to be lowest in energy for each isomer has always been observed experimentally. However, the conformer populations are certainly not in equilibrium at the rotational temperature (1.0–1.5 K).

Table III includes experimentally determined $\tilde{A}$-$\tilde{X}$ energy separations. The smallness of these separations for the C_s-symmetry structures calls for further investigation about possible pseudo-Jahn-Teller interactions, since it is possible for the two potential energy surfaces (PESs) to distort substantially upon consideration of such vibronic effects. For 2-propoxy, the T conformer of 1-propoxy and the T_1T_2 conformer of 1-butoxy the geometry optimizations started from C_1-symmetry structures and resulted in 0.4, 1.9, and 7.4 cm^{-1} stabilization, respectively, as compared to the optimized C_s-symmetry point of the $\tilde{X}$ potential energy curve. Although single-reference theories are not accurate enough to reliably calculate the stabilization energy, owing to artificial symmetry breaking problems,[15,16] these results may be used as a means to obtain a rough qualitative picture of trends in the alkoxy radicals. Methodologies like the equation-of-motion ionization potentials coupled cluster singles and doubles[17,18] avoid problems of artificial symmetry breaking but they become computationally expensive as the size of the molecule increases. For the aforementioned C_s structures, we conclude from the calculations no serious distortion of the PES of the ground state is expected, hence one would not expect vibrational progressions other than the totally symmetric ones to be promoted significantly in the excited electronic state.

Finally it is worth mentioning a possibly obvious but quite important point. In percentage terms we expect the calculation of the vibrational frequencies of both the $\tilde{X}$ and $\tilde{A}$ states to be much more accurate than the $\tilde{A}$-$\tilde{X}$ separation. The problem with the latter prediction, of course, is that the $\tilde{A}$-$\tilde{X}$ difference is very small compared to the computed absolute energies of the states, which means that even if the absolute error in the states' energies is small the error in the difference can be relatively large. To get accurate $\tilde{A}$-$\tilde{X}$ values would require a very large basis set with high-quality (correlation) methods. One could also have to take into account all the auxiliary corrections (e.g., relativistic, Born-Oppenheimer breakdown, core-correlation, anharmonic zero-point energy corrections).

B. DF observations

Figures 2 and 3 show survey scans of LIF spectra of the primary and secondary alkoxy radicals, respectively. Laser excited DF spectra were recorded for a number of vibronic bands labeled by the letters shown in the corresponding LIF traces.

In principle, the DF spectra provide a direct experimental way of obtaining the energy difference between the $\tilde{A}$ and

TABLE V. The calculated lowest 23 vibrational frequencies (in cm^{-1}) of the T_1T_2 conformer of 1-butoxy radical in its ground electronic state as obtained at the B3LYP/6-31+G* level of theory.

Assignment	$\tilde{X},T_1T_2$ B3LYP[a]	CO stretch	CCO deformation[b]	Q[c]
ν_{14}	1435(a')			CC stretch, CH_3 rock
ν_{15}	1413(a')	Small		CH_3, CH_2 rock, CC stretch
ν_{16}	1393(a')	Small		CH_3, CH_2 rock, CC stretch
ν_{17}	1369(a')	Small		CH_3, CH_2 rock, CCC bend
ν_{18}	1339(a'')			CH_3, CH_2 rock
ν_{19}	1304(a'')			CH_3, CH_2 rock
ν_{20}	1282(a')	Small		CH_3, CH_2 rock
ν_{21}	1227(a'')			CH_3, CH_2 rock
ν_{22}	1133(a')		Medium	CH_3, CH_2 rock, CCC bend
ν_{23}	1079(a')	Large		CH_3, CH_2 rock, CC stretch
ν_{24}	1061(a')	Small		CC stretch
ν_{25}	1006(a'')		Small	CH_3, CH_2 rock, CC stretch
ν_{26}	995(a')	Medium	Large	CH_3, CH_2 rock, CC stretch
ν_{27}	914(a')		Medium	CH_3, CH_2 rock, CC stretch
ν_{28}	849(a'')			CH_3, CH_2 rock
ν_{29}	746(a'')			CH_3, CH_2 rock
ν_{30}	467(a')		Large	CH_2 torsion, CCC bend
ν_{31}	391(a')		Medium	CH_2 torsion, CCC bend
ν_{32}	361(a'')		Medium	CH_3, CH_2 torsion
ν_{33}	244(a'')			CH_3, CH_2 torsion
ν_{34}	185(a')			Backbone flex
ν_{35}	114(a'')			Backbone flex
ν_{36}	106(a'')			Backbone flex

[a]The unscaled harmonic frequencies were obtained at the C_1-symmetry minimum, and their symmetries under the C_s point group are included in parenthesis. The labeling of the vibrational mode follows the Mülliken notation scheme (Ref. 14).

[b]For a' symmetry modes the CCO deformation is an in-plane bend and for a'' symmetry modes it is an out-of-plane twist.

[c]The contributions of various internal coordinates Q to the normal mode indicated in the first column are listed, other than the CO stretch or CCO deformation which are listed in the preceding two columns with a qualitative indication of their magnitude.

$\tilde{X}$ states. However, to accurately determine the origin of the $\tilde{A}$ state, one needs to uniquely identify the $\tilde{B}$-$\tilde{A}$ origin band among bands belonging to the vibrationally excited levels of the $\tilde{X}$ ($\tilde{A}$) states, the latter of course giving valuable information about the vibrational frequencies of these states. Our assignments were aided with quantum chemical predictions of both the energy separation of these two states and the vibrational levels for the ground electronic state. From the present and previous[12] computational work, we have found the PES for the close-lying $\tilde{A}$ state to be similar to that of the ground state. Hence the vibrational frequencies are not expected to differ greatly between these two electronic states, with the exception of some possible frequencies that exhibit pseudo-Jahn-Teller activity for the C_s conformers.[12]

It is pertinent to mention the following additional principles upon which we base our assignments of the vibrational levels of the $\tilde{X}$ and $\tilde{A}$ states:(i) under C_s-symmetry (or near C_s symmetry), only the totally symmetric fundamentals are electronically allowed and therefore these are expected to exhibit the strongest fluorescence intensity; (ii) only vibrations of CO stretch or CCO deformation (bend or twist), or vibrations coupled to those, are anticipated to have significant nondiagonal Franck-Condon factors, since the $\tilde{B}$, $\tilde{A}$, and $\tilde{X}$ potentials are quite similar along other modes, as the electronic transition is localized on the O atom.

1. 1-Propoxy

For 1-propoxy, the DF spectra were recorded by pumping bands *A* and *B* shown in Fig. 2. Band *A* has been identified by detailed rotational analysis[5] as the origin of the *G* conformer and band *B* is the origin of the *T* conformer. These DF spectra are shown in Fig. 4, while Fig. 5 shows an expanded view of their DF spectra within 1700 cm^{-1} redshifted from the pumping frequency.

The *T* conformer of 1-propoxy is a nominally C_s-symmetry structure and therefore one would expect the totally symmetric fundamental frequencies to dominate in the DF spectrum. It is the CO stretch motion that is expected to exhibit the strongest fluorescence intensity, thus the strongest transitions should be assigned to CO stretch vibrations. A strong progression in the $\tilde{X}$ state of the *T* conformer can immediately be identified with a 1-0 vibrational interval of 1050 cm^{-1} redshifted from the $\tilde{X}$ state origin located at 0 cm^{-1}. We attribute this main vibrational progression to ν_{18}, as this mode has the strongest CO stretch character among all of the modes (see Table IV). Mode ν_{19} involves significant but less participation of the CO stretch motion than ν_{18} and that is analogously reflected in the DF spectrum via the fluorescence intensity of the corresponding 1-0 band assigned to the 1017 cm^{-1} peak in Table VIII.

Based upon the match with the theoretically calculated

TABLE VI. The calculated lowest 16 vibrational frequencies (in cm^{-1}) of 2-propoxy radical in its ground electronic state as obtained at the B3LYP/6-31+G* level of theory.

Assignment	$\tilde{X}$ B3LYP[a]	CO stretch	$(C)_2$CO deformation[b]	Q[c]
ν_{12}	1428(a')			CH_3 rock, CC stretch
ν_{13}	1404(a'')			CH_3, CH rock, CC stretch
ν_{14}	1261(a')	Large		CH_3, CH rock
ν_{15}	1207(a')	Medium		CH_3, CH rock
ν_{16}	1165(a'')			CH_3, CH rock
ν_{17}	1069(a'')		Large	CH_3 rock, CC stretch
ν_{18}	1054(a')	Small		CH_3, CH rock
ν_{19}	984(a')	Large		CH_3 rock
ν_{20}	921(a'')			CH_3 rock, CC stretch
ν_{21}	888(a'')			CH_3, CH rock
ν_{22}	809(a')	Medium		CC stretch
ν_{23}	453(a')		Medium	CCC bend
ν_{24}	390(a'')		Large	
ν_{25}	359(a')		Small	CCC bend
ν_{26}	244(a')			CH_3 torsion
ν_{27}	197(a'')			CH_3 torsion

[a]The unscaled harmonic frequencies were obtained at the C_1-symmetry minimum and their symmetries under the C_s point group are included in parenthesis. The labeling of the frequencies follows the Mülliken notation scheme.

[b]For a' symmetry modes the $(C)_2$CO (or HCO) deformation is an in-plane bend and for a'' symmetry modes it is an out-of-plane twist.

[c]The contributions of various internal coordinates Q to the normal mode indicated in the first column are listed, other than the CO stretch or CCO deformation which are listed in the preceding two columns with a qualitative indication of their magnitude.

TABLE VII. The calculated lowest 22 vibrational frequencies (in cm^{-1}) of the $G+$ conformer of 2-butoxy radical in its ground electronic state as obtained at the B3LYP/6-31+G* level of theory.

Assignment	$\tilde{X}, G+$ B3LYP[a]	CO stretch	$(C)_2$CO deformation	Q[b]
ν_{15}	1432			CH_3, CH_2 rock, CC stretch
ν_{16}	1418			CH_3, CH_2 rock, CC stretch
ν_{17}	1353	Small		CH_3, CH_2 rock, CC stretch
ν_{18}	1311	Small		CH_3, CH_2 rock
ν_{19}	1244	Large		CH_3, CH_2 rock, CC stretch
ν_{20}	1194	Large		CH_3, CH_2 rock, CC stretch, CCC bend
ν_{21}	1165	Small		CH_3, CH_2 rock, CC stretch
ν_{22}	1067	Small		CH_3, CH_2 rock, CC stretch
ν_{23}	1059		Medium	CH_3, CH_2 rock, CC stretch
ν_{24}	1030	Large	Large	CH_3, CH_2 rock, CC stretch
ν_{25}	1000			CH_3, CH_2 rock, CC stretch
ν_{26}	936	Large		CH_3, CH_2 rock, CC stretch
ν_{27}	927	Medium	Medium	CH_3, CH_2 rock, CC stretch
ν_{28}	794		Medium	CH_3, CH_2 rock, CC stretch
ν_{29}	773	Medium		CH_3, CH_2 rock, CC stretch
ν_{30}	468		Large	CCC bend
ν_{31}	431		Large	CCC bend
ν_{32}	365		Large	CCC bend
ν_{33}	247			CCC bend
ν_{34}	216			CH_3 torsion, CCC bend
ν_{35}	208			CH_3 torsion
ν_{36}	95			Backbone flex

[a]Unscaled harmonic frequencies. The labeling of the vibrational modes follows the Mülliken notation scheme (Ref. 14) for a C_1 molecule.

[b]The contributions of various internal coordinates Q to the normal mode indicated in the first column are listed, other than the CO stretch or CCO deformation which are listed in the preceding two columns with a qualitative indication of their magnitude.

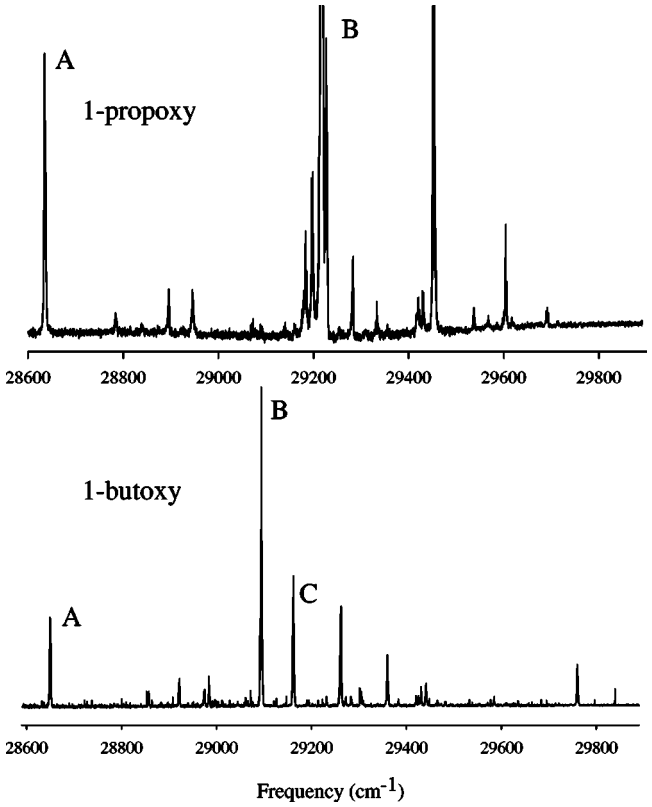

FIG. 2. Survey scans of the LIF spectra of the primary radicals. The line labeled *B* in 1-propoxy extends off-scale so as to show more clearly the weaker transitions.

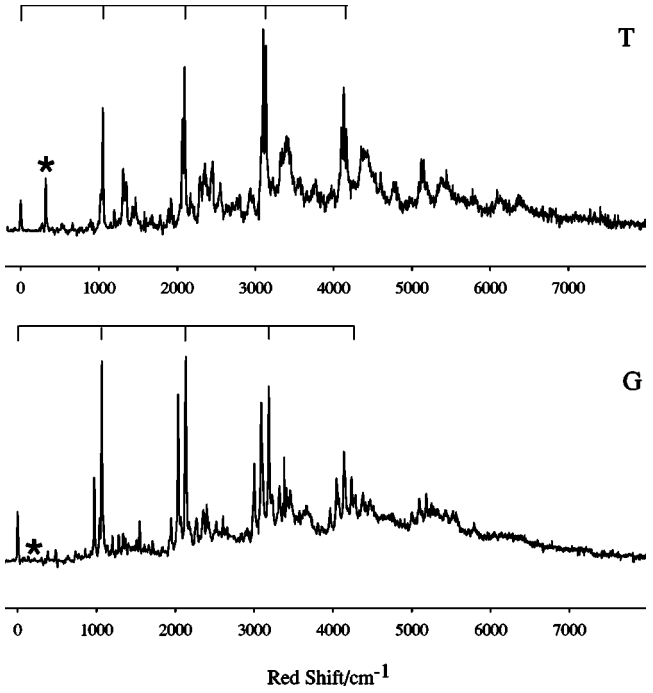

FIG. 4. DF spectra of the *T* and *G* conformations of 1-propoxy radical. The top trace was obtained by pumping band *B* (Fig. 2), the origin of the *T* conformer, at 29 218 cm^{-1} while the bottom trace was obtained by pumping band *A* (Fig. 2), the origin of the *G* conformer, at 28 634 cm^{-1}. The *x* axis indicates (red) shift from the pump frequency. Assigned members of the predominant CO stretch progression, ν_{18} (*T* and *G*), are indicated by ticks on the top horizontal bar while the * indicates the line assigned to the $\tilde{A}$-$\tilde{X}$ origin transition. The intensities are not corrected for the grating efficiency and the camera sensitivity curves. The experimental resolution was 15 cm^{-1}.

frequencies (see Table VIII), we have assigned several other, lower intensity, totally symmetric fundamentals to the $\tilde{X}$ state. The bands at 274 (ν_{25}^{X}), 527 (ν_{23}^{X}), 895 (ν_{21}^{X}), and 1060 (ν_{17}^{X}) cm^{-1} have been assigned to levels with reasonably large CCO internal coordinate contributions. This assigns all totally symmetric fundamentals calculated to be below 1200 cm^{-1}. The theoretical calculations have shown that within 1300–1450 cm^{-1} there are four totally symmetric vibrational modes that all involve some CO stretch and/or CCO bend movement in their motion. Only two of those, likely ν_{12}^{X} and ν_{11}^{X}, appear obviously in the spectrum and their peaks are at 1426 and 1460 cm^{-1}, respectively. Their proximity may result in intensity borrowing between these bands. Nontotally symmetric fundamentals are not allowed

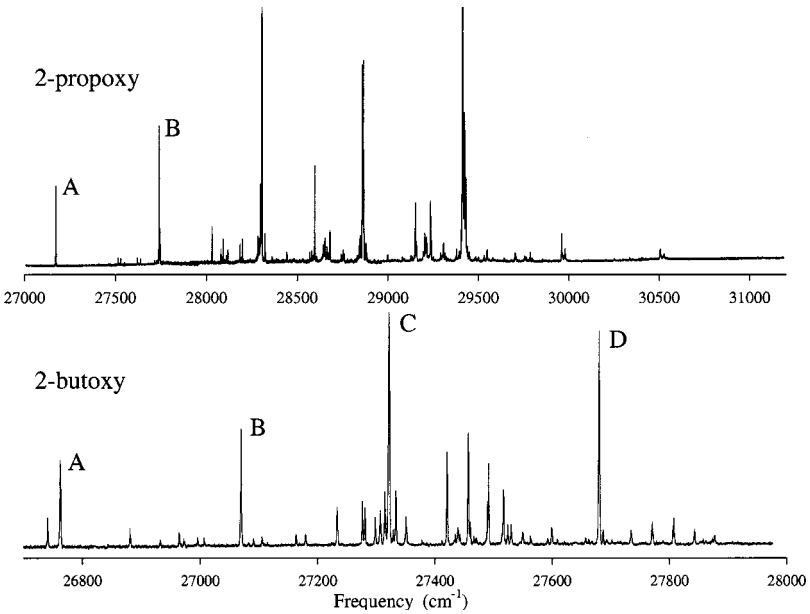

FIG. 3. Survey scans of the LIF spectra of the secondary alkoxies. Note the difference in frequency scales.

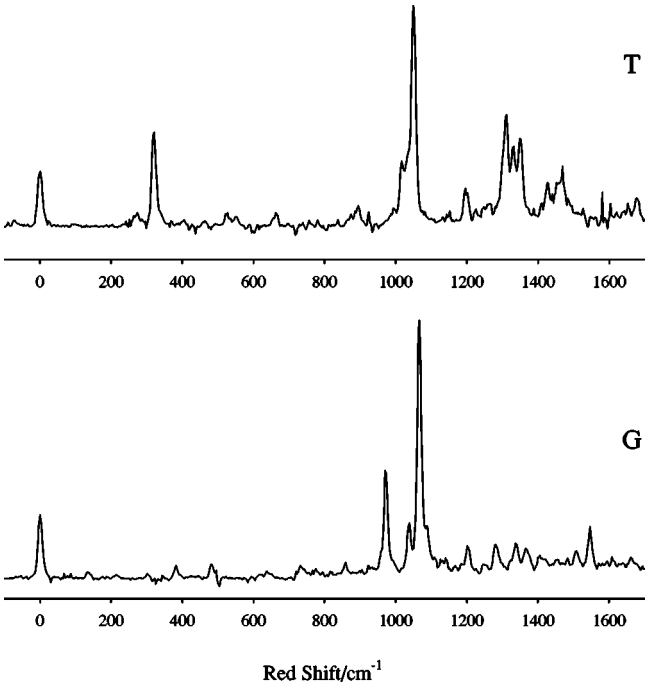

FIG. 5. An expanded view of the DF spectra of the *T* and *G* conformations of 1-propoxy radical. The top trace was obtained by pumping band *B* (Fig. 2), the origin of the *T* conformer, at 29 218 cm^{-1} while the bottom trace was obtained by pumping band *A* (Fig. 2), the origin of the *G* conformer, at 28 634 cm^{-1}. The *x* axis indicates (red) shift from the pump frequency. The intensities are not corrected for the grating efficiency and the camera sensitivity curves. The experimental resolution was 15 cm^{-1}.

by symmetry considerations, and their overtones, though are not prohibited, are expected to be generally weak. However, the first overtone of ν_{24}^X, which is the most pseudo-Jahn-Teller-active vibrational mode, may be a suitable candidate for the band appearing at 662 cm^{-1}.

By analogy with the reasoning for the $\tilde{X}$ state assignments, we anticipate the totally symmetric CO stretch modes to have large fluorescence intensities in the transition to the $\tilde{A}$ state as well. However, the identification of the vibrationless level of the $\tilde{A}$ state is the first step for assignments of the $\tilde{A}$ state vibrational levels. As Fig. 4 shows, we have identified the band at 321 cm^{-1} as the vibrationless level of the $\tilde{A}$ state. The two theoretically calculated $\tilde{X}$ state vibrational frequencies closest to this value that are expected to show fluorescence intensity correspond to 270 and 475 cm^{-1} (see Table IV). In addition to the mismatch in frequency (which is large but not impossible given possible computational errors), the magnitude of the observed fluorescence intensity discourages the assignment of this band to either of these two vibrations. Our theoretically calculated $\tilde{A}$-$\tilde{X}$ separation quoted in Table III, while as noted in Sec. III A, subject to considerable uncertainty, is consistent with this assignment. Similar to the $\tilde{X}$ state, a vibrational progression associated with the ν_{18} mode appears in the $\tilde{A}$ state, with an energy interval of 1011 cm^{-1} from the above identified $\tilde{A}$ state origin. Using the other $\tilde{X}$ state assignments as a guide, we have assigned the bands at 552, 844, 1193, 1311, and 1352 cm^{-1} to the following modes of the $\tilde{A}$ state: ν_{25}^A, ν_{23}^A, ν_{21}^A, ν_{19}^A, and ν_{17}^A, respectively. It should be pointed out that there are vibrational progressions associated with ν_{17} and ν_{19} in both the $\tilde{X}$ and $\tilde{A}$ states, probably arising via intensity borrowing among the closely energy spaced totally symmetric ν_{17}, ν_{18}, and ν_{19} levels.

TABLE VIII. Assignment of the DF spectrum of the *T* conformer of 1-propoxy radical. The vibrational assignment is made for the emission pumping bands shown in Fig. 5.

Assignment	Frequency		
	Predicted[a]		Experimental[b]
	$\tilde{X}$	$\tilde{A}$	
ν_0^X			0
ν_{25}^X	270		274
ν_0^A			321
			340[c]
ν_{23}^X	475		527
$\nu_{25}^A+\nu_0^A$		591	552
$2\nu_{24}^X$	614		662
$\nu_{23}^A+\nu_0^A$		796	844
ν_{21}^X	889		895
ν_{19}^X	1034		1017
ν_{18}^X	1074		1050
ν_{17}^X	1128		1060
$\nu_{21}^A+\nu_0^A$		1210	1193
$\nu_{19}^A+\nu_0^A$		1355	1311
$\nu_{18}^A+\nu_0^A$		1395	1332
$\nu_{17}^A+\nu_0^A$		1449	1352
ν_{12}^X	1414		1426
ν_{11}^X	1436		1460

[a]Unscaled frequencies computed at the B3LYP/6-31+G* level of theory (in cm^{-1}). The vibrational levels of the $\tilde{A}$ state were estimated by adding the experimentally observed vibrationless level of the $\tilde{A}$ state (denoted as ν_0^A) to the corresponding theoretically predicted frequencies under the column of assignment. The assignment was made on the grounds that the PES for the lowest two energy states does not change considerably.

[b]Experimentally observed vibrational bands (in cm^{-1}) relative to the vibrationless level of the $\tilde{X}$ state ν_0^X.

[c]Possible shoulder.

The *G* conformer of 1-propoxy is a C_1-symmetry structure and hence one may not preclude the appearance of any of its vibrations in the DF spectrum. However, again it is the CO stretch character that carries most of the oscillator strength, therefore the strongest transitions should be connected with the CO stretch vibrations. In the DF spectrum of the *G* conformer (see Fig. 5), a strong progression in the $\tilde{X}$ state can immediately be identified with a vibrational spacing of 1066 cm^{-1}, which as in the *T* conformer, we attribute to ν_{18} (see Table 2 of the Supplementary Material). The second strongest transition below 1700 cm^{-1} peaks at 973 cm^{-1} and is assigned to ν_{19}, which also has significant CO stretch character. Table IX presents a number of assigned vibrational bands based upon matches with calculated frequencies. Indeed in this C_1-symmetry molecule, there appears to be a peak assignable to every vibrational mode expected below 1200 cm^{-1}.

The bands appearing at 1337, 1365, and 1546 cm^{-1} have been assigned as combination bands of one quantum of excitation of ν_{18}^X with, respectively, two quanta of ν_{27}^X, one quantum of ν_{25}^X, and one quantum of ν_{23}^X. The corresponding

TABLE IX. Assignment of the DF spectrum of the *G* conformer of 1-propoxy radical. The vibrational assignment is made for the emission pumping bands shown in Fig. 5.

Assignment	Frequency		
	Predicted[a]		Experimental[b]
	$\tilde{X}$	$\tilde{A}$	
ν_0^X			0
ν_{27}^X	125		135
ν_0^A			214
ν_{25}^X	286		302
ν_{24}^X	305		383
ν_{23}^X	496		485
$\nu_{23}^X+\nu_{27}^X$	621		650
ν_{22}^X	788		743
ν_{21}^X	867		859
ν_{19}^X	995		973
ν_{17}^X	1114		1039
ν_{18}^X	1092		1066
$\nu_{19}^A+\nu_0^A$		1209	1204
$\nu_{17}^A+\nu_0^A$		1328	1254
$\nu_{18}^A+\nu_0^A$		1306	1282
$\nu_{18}^X+2\nu_{27}^X$	1342		1337
$\nu_{18}^X+\nu_{25}^X$	1378		1365
$\nu_{18}^X+\nu_{23}^X$	1588		1546
$2\nu_{19}^X$	1990		1947
$2\nu_{17}^X$	2228		2033
$2\nu_{18}^X$	2184		2132
$2\nu_{19}^A+\nu_0^A$		2204	2168
$2\nu_{17}^A+\nu_0^A$		2442	2251
$2\nu_{18}^A+\nu_0^A$		2398	2350
$2\nu_{18}^X+2\nu_{27}^X$	2434		2399
$2\nu_{18}^X+\nu_{25}^X$	2470		2427
$2\nu_{18}^X+\nu_{23}^X$	2680		2603
$3\nu_{19}^X$	2985		3000
$3\nu_{17}^X$	3342		3089
$3\nu_{18}^X$	3276		3183
$3\nu_{19}^A+\nu_0^A$		3199	3223
$3\nu_{17}^A+\nu_0^A$		3556	3316
$3\nu_{18}^A+\nu_0^A$		3490	3409

[a]Unscaled harmonic frequencies computed at the B3LYP/6-31+G* level of theory (in cm^{-1}).

[b]Experimentally observed vibrational bands (in cm^{-1}) relative to the vibrationless level of the $\tilde{X}$ state ν_0^X.

combination bands but with two quanta of excitation of ν_{18}^X lead to the appearance of the following peaks in the DF spectrum: 2399, 2427, and 2603 cm^{-1}. This repeated pattern of observed frequencies in the energy region higher than 2000 cm^{-1} of redshift strongly validates our previous assignments of the combination bands with ν_{18}^X.

One notes that unlike the *T* conformer, in the *G* conformer the $\tilde{A}$ state origin (nor excited vibrations) does not distinctly appear in the spectrum. The theoretical predictions (see Table III) indicate that the $\tilde{A}$ state origin lies very close to the $\tilde{X}$ state origin. The experimental resolution could be insufficient to resolve the $\tilde{B}$-$\tilde{A}$ and $\tilde{B}$-$\tilde{X}$ transitions. In this case the experimental resolution places an upper limit on the $\tilde{A}$-$\tilde{X}$ separation of $\lesssim 15\ cm^{-1}$.

A second possibility would be that the $\tilde{A}$ state origin appears at a resolvable separation from that of the $\tilde{X}$ state but with considerably diminished intensity. Whereas in the *T* conformation one can easily identify the $\tilde{A}$ state origin as well as the vibrational structures built upon the bands belonging to it, in the *G* conformer it is difficult to make comparable assignments. What is different in the later case is that the symmetry is lower. A single argument shows that a strongly diminished $\tilde{A}$ state origin intensity is possible. Assume for the $C_s(T)$ conformer the $\tilde{B}$-$\tilde{A}$ and $\tilde{B}$-$\tilde{X}$ intensities are exactly the same. Further assume that the electronic eigenfunctions of the *G* conformer are just the symmetric and antisymmetric linear combinations of the *T* state eigenfunctions. Both assumptions are qualitatively reasonable and together yield the result that the $\tilde{B}$-$\tilde{X}$ intensity increases by a factor of 2 going from the *T* to *G* conformer while the $\tilde{B}$-$\tilde{A}$ intensity exactly goes to zero.

Of course we do not expect this simple model to be completely correct and we also expect some variation in the $\tilde{B}$-$\tilde{X}$ and $\tilde{B}$-$\tilde{A}$ intensities along the strong CO stretch progression. Indeed for the alkoxies as a whole the $\tilde{B}$-$\tilde{A}$ transition seems to slightly increase in intensity for higher CO stretch quanta. It therefore seems reasonable to look for $\tilde{B}$-$\tilde{A}$ CO stretch bands in the vicinity of the corresponding $\tilde{B}$-$\tilde{X}$ bands.

The triplet of bands ν_{19}^X, ν_{18}^X, and ν_{17}^X exhibit high fluorescence intensities in the $\tilde{X}$ state, hence they are good candidates for the assignment of their analog in the $\tilde{A}$ state. Indeed, the peaks appearing at 1204, 1254, and 1282 cm^{-1} could possibly be identified as ν_{19}^A, ν_{17}^A, and ν_{18}^A, respectively. All three of these $\tilde{A}$ state bands show a profile of intensities that appear decreased in a proportional way with respect to corresponding $\tilde{X}$ state ones. From these lines one would deduce an $\tilde{A}$-$\tilde{X}$ separation of 214 cm^{-1}. Moreover, a peak displaced from the $\tilde{B}$-$\tilde{X}$ origin by 214 cm^{-1} actually appears in the DF spectrum albeit with a very low intensity. Going to a higher-frequency region, we identified the first overtones of ν_{19}^X, ν_{17}^X, and ν_{18}^X peaking at the frequencies of 1947, 2033, and 2132 cm^{-1}, respectively. The same pattern as before in the $\tilde{X}$ state is consistently reproduced in the $\tilde{A}$ state, i.e., the peaks at 2168, 2251, and 2350 cm^{-1} may be assigned as their corresponding $\tilde{A}$ state bands. The second overtones of the same modes appearing at 3000 (ν_{19}^X), 3089 (ν_{17}^X), and 3183 (ν_{18}^X) cm^{-1} exhibit fluorescence intensity, with corresponding bands in the $\tilde{A}$ state at 3223, 3316, and 3409 cm^{-1}, respectively. Obviously the poor Franck-Condon factors for the $\tilde{A}$ state make it impossible for the majority of the vibrational modes to appear in the spectrum save for the strongest modes identified in the $\tilde{X}$ state. We consider the determination of the $\tilde{A}$-$\tilde{X}$ separation of 214 cm^{-1} to be likely correct. However, the large number of vibrational modes possibly active in the *G* conformer, makes it impossible to definitely affirm this value or rule out that the $\tilde{A}$-$\tilde{X}$ separation is just too small to be resolved.

The largest discrepancies between the calculated harmonic frequencies and the experimentally observed anharmonic frequencies lie, for the *T* conformer, with ν_{17}^X, ν_{18}^A, and ν_{17}^A while for the *G* conformer with ν_{24}^X and ν_{17}^X. We

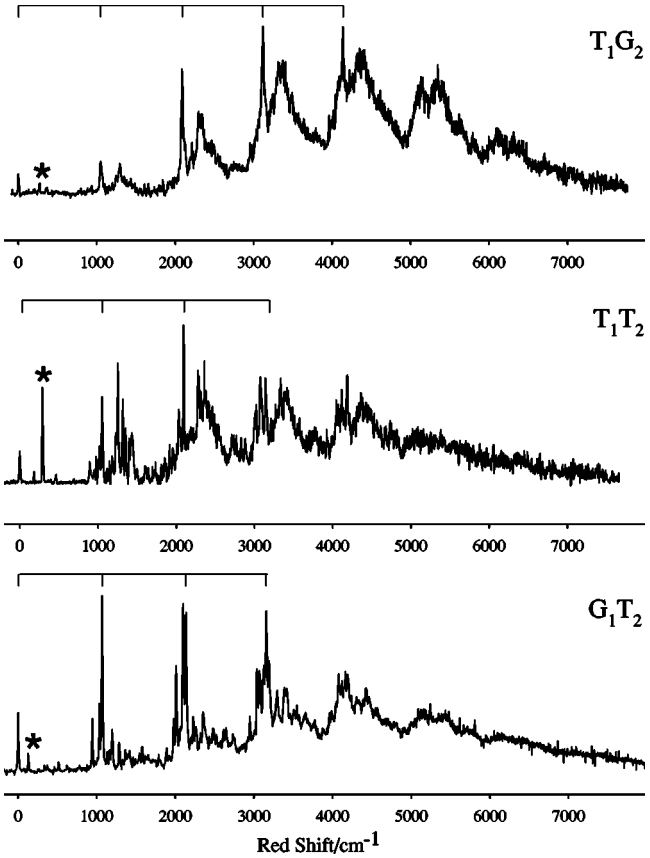

FIG. 6. DF spectra of the T_1G_2, T_1T_2, and G_1T_2 conformations of 1-butoxy radical. The top trace was obtained by pumping band *C* (Fig. 2), the origin of the T_1G_2 conformer, at 29 164 cm^{-1}, the middle trace was obtained by pumping band *B* (Fig. 2), the origin of the T_1T_2 conformer, at 29 095 cm^{-1} while the bottom trace by pumping band *A* (Fig. 2), the origin of the G_1T_2 conformer, at 28 649 cm^{-1}. The *x* axis indicates (red) shift from the pump frequency. Assigned members of the predominant CO stretch progression, $\nu_{23}(T_1T_2)$, $\nu_{24}(T_1G_2)$, and $\nu_{23}(G_1T_2)$, are indicated by ticks on the top horizontal bar while the* indicates the line assigned to the $\tilde{A}$-$\tilde{X}$ origin transition. The intensities are not corrected for the grating efficiency and the camera sensitivity curves. The experimental resolution was 15 cm^{-1}.

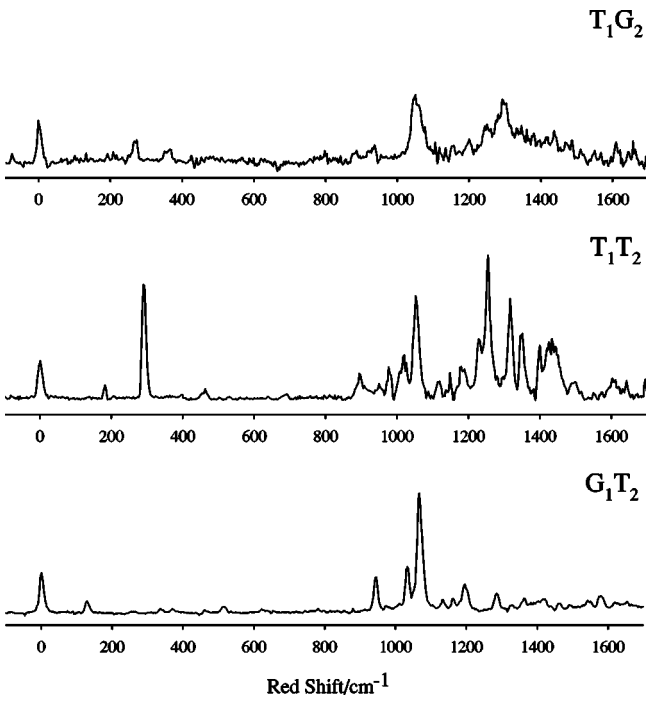

FIG. 7. An expanded view of the DF spectra of the T_1G_2, T_1T_2, and G_1T_2 conformations of 1-butoxy radical. The top trace was obtained by pumping band *C* (Fig. 2), the origin of the T_1G_2 conformer, at 29 164 cm^{-1}, the middle trace was obtained by pumping band *B* (Fig. 2), the origin of the T_1T_2 conformer, at 29 095 cm^{-1} while the bottom trace by pumping band *A* (Fig. 2), the origin of the G_1T_2 conformer, at 28 649 cm^{-1}. The *x* axis indicates (red) shift from the pump frequency. The intensities are not corrected for the grating efficiency and the camera sensitivity curves. The experimental resolution was 15 cm^{-1}.

need to recognize that while the B3LYP methodology is generally a cost-effective procedure for predicting reliable vibrational frequencies, its results are obtained by use of the harmonic approximation. Neither possible anharmonicity effects (probably ν_{17}^X of *T* and *G* conformers) nor vibronic coupling interactions between the $\tilde{X}$ and $\tilde{A}$ states (ν_{25}^A and $2\nu_{24}^X$ of the *T* conformer) are incorporated in the vibrational frequency calculations. In addition, mechanisms like intensity borrowing between energetically closely spaced bands (e.g., ν_{19}^A, ν_{18}^A, and ν_{17}^A of the *T* conformer) of the same symmetry may not be completely described by such calculations.

2. 1-Butoxy

For 1-butoxy, the DF spectra were recorded by pumping bands *A*, *B*, and *C* shown in Fig. 2. Band *A* has been identified[6] as the origin of the G_1T_2 conformer, band *B* is the origin of the T_1T_2 conformer, and band *C* of T_1G_2. The DF spectra of these species are shown in Fig. 6, while Fig. 7 shows an expanded view of their DF spectra up to $\approx$1600 cm^{-1} redshifted from the pumping frequency.

Using our experience with the *T* conformer of 1-propoxy, the vibrational interval of 1052 cm^{-1} measured from the $\tilde{X}$ state origin may be associated with the CO stretch progression in the $\tilde{X}$ state for the T_1T_2 conformation of 1-butoxy. Since the vibrational mode ν_{23} encompasses the largest CO stretch character we assign this band and the higher members of the progression to this mode. On the grounds of matching well with the theoretically calculated frequencies (see Table X), the following low-intensity, totally symmetric fundamentals were assigned in the $\tilde{X}$ state: the bands at 395 (ν_{31}^X), 950 (ν_{27}^X), and 1116 (ν_{22}^X) cm^{-1} involve medium CCO deformation in their motion, and the band at 463 (ν_{30}^X) cm^{-1} large CCO deformation. The band at 976 cm^{-1} is identified as ν_{26}^X, a mode with moderate CO stretch and large CCO bend character. The band at 183 cm^{-1} was assigned to ν_{34}^X and is a backbone flex mode. The vibration ν_{24} involves a small amount of CO stretch character and is assigned to the peak at 1017 cm^{-1} in the $\tilde{X}$ state. Finally, the bands peaking at 1279 (ν_{20}^X), 1425 (ν_{17}^X), and 1437 (ν_{16}^X) cm^{-1} likely correspond to modes involving small CO and small CCO deformation.

Following the same arguments for the assignment of the $\tilde{A}$ state origin in the *T* conformer of 1-propoxy (and within the expectedly large interval of uncertainty of our theoretical calculations quoted in Table III), we have identified the peak

TABLE X. Assignment of the DF spectrum of the T_1T_2 conformer of 1-butoxy radical. The vibrational assignment is made for the emission pumping bands shown in Fig. 7.

Assignment	Frequency		
	Predicted[a]		Experimental[b]
	$\tilde{X}$	$\tilde{A}$	
ν_0^X			0
ν_{34}^X	185		183
ν_0^A			292
ν_{31}^X	391		395
(ν_{30}^X and $\nu_{34}^A+\nu_0^A$)[c]	467	477	463
$\nu_{31}^A+\nu_0^A$		683	688
$\nu_{30}^A+\nu_0^A$		759	895
ν_{27}^X	914		950
ν_{26}^X	995		976
ν_{24}^X	1061		1017
ν_{23}^X	1079		1052
(ν_{22}^X and $\nu_{27}^X+\nu_{34}^X$)[c]	1133 and 1099		1116
$\nu_{26}^X+\nu_{34}^X$	1180		1148
$\nu_{24}^X+\nu_{34}^X$	1246		1191
$\nu_{27}^A+\nu_0^A$		1206	1229
$\nu_{26}^A+\nu_0^A$		1287	1255
ν_{20}^X	1282		1279
$\nu_{24}^A+\nu_0^A$		1353	1319
$\nu_{23}^A+\nu_0^A$		1371	1348
$\nu_{22}^A+\nu_0^A$		1425	1400
(ν_{17}^X and $\nu_{27}^A+\nu_{34}^A+\nu_0^A$)[c]	1369	1391	1425
ν_{16}^X	1393		1437
(ν_{15}^X and $\nu_{26}^A+\nu_{34}^A+\nu_0^A$)[c]	1413	1472	1445
$\nu_{24}^A+\nu_{34}^A+\nu_0^A$		1538	1493
$\nu_{20}^A+\nu_0^A$		1574	1572

[a]See footnote a of Table VIII.

[b]Experimentally observed vibrational bands (in cm^{-1}) relative to the vibrationless level of the $\tilde{X}$ state ν_0^X.

[c]The experimental bands may have dual assignments.

at 292 cm^{-1} as the vibrationless level of the $\tilde{A}$ state. The band redshifted from it by 1056 cm^{-1} (at 1348 cm^{-1}) is correlated with the strong CO stretch character vibration ν_{23}, a mode that also leads a vibrational progression in the $\tilde{A}$ state. By reference to our $\tilde{X}$ state assignments, we make similar assignments in the $\tilde{A}$ state, as detailed in Table X.

While the T_1T_2 conformer of 1-butoxy is a near-C_s symmetry structure, the geometry of the T_1G_2 conformation is characterized by significant departure from the C_s-symmetry reference structure. The CO stretch progression in the $\tilde{X}$ state is easily identifiable in Fig. 6. The vibrational 1-0 spacing of the first number of this relatively strong CO stretch progression is 1050 cm^{-1} and we associated ν_{24} with strong CO stretch character mode with this band. (See Table 5 of the Supplementary Material.) Using as a reference of the calculated frequencies, we make additional assignments of the lower intensity bands in the $\tilde{X}$ state. The weak peaks at 79 (ν_{36}^X) and 101 (ν_{35}^X) cm^{-1} are characterized as vibrations that exhibit backbone flex motions, and the peak at 208 (ν_{34}^X) cm^{-1} is characterized by a mode of CH_3 torsion and CCC bend. The bands peaking at 351 (ν_{32}^X) and 484 (ν_{31}^X) cm^{-1} are attributed to modes involving large CCO deformation in their motion, the peaks at 798 (ν_{28}^X), 886 (ν_{27}^X), and 930 (ν_{26}^X) cm^{-1} correspond to modes containing the internal coordinates of medium-sized CCO and small-sized CO movement, medium CCO deformation and medium CO/large CCO motion, respectively. Mode ν_{23}^X involves medium CCO and small CO movements and reasonably correlates with a peak at 1071 cm^{-1} and mode ν_{22}^X is characterized by a medium CO movement and corresponds to the peak appearing at 1117 cm^{-1}. The bands centered at 1135 (ν_{21}^X), 1244 (ν_{20}^X), 1300 (ν_{19}^X), and 1338 (ν_{18}^X) are built upon vibrational modes that include small amounts of CO stretch character in their motion.

The assignment of the $\tilde{A}$ state origin is based on the consideration that the strong CO stretch progression appearing in the $\tilde{X}$ state should also appear in the $\tilde{A}$ state. The band at 1300 cm^{-1} is most likely the first member of the CO stretch progression in the $\tilde{A}$ state, and is likewise assigned to ν_{24}^A. This assignment identifies the origin of the $\tilde{A}$ state at 271 cm^{-1} above the $\tilde{X}$ state. Other observed peaks at frequencies lower than 1600 cm^{-1} that may be assigned to the $\tilde{A}$ state are given in Table XI.

For the G_1T_2 conformation, a pronounced vibrational progression with a 1-0 interval of 1067 cm^{-1} is attributed to the CO stretch motion in the $\tilde{X}$ state and is assigned to ν_{23}, the character of which is predominantly the CO stretch movement (see Table 6 of the Supplementary Material). Based upon the match with the calculated frequencies, we assigned the following low-intensity bands: 259 (ν_{33}^X) cm^{-1} corresponds to a CH_3/CH_2 torsion and CCC bend mode, 337

TABLE XI. Assignment of the DF spectrum of the T_1G_2 conformer of 1-butoxy radical. The vibrational assignment is made for the emission pumping bands shown in Fig. 7.

Assignment	Frequency		
	Predicted[a]		Experimental[b]
	$\tilde{X}$	$\tilde{A}$	
ν_0^X			0
ν_{36}^X	97		79
ν_{35}^X	117		101
ν_{34}^X	208		208
ν_0^A			271
(ν_{32}^X and $\nu_{36}^A+\nu_0^A$)[c]	346	368	351
$\nu_{35}^A+\nu_0^A$		388	367
(ν_{31}^X and $\nu_{34}^A+\nu_0^A$)[c]	474	479	484
$\nu_{32}^A+\nu_0^A$		617	621
$\nu_{31}^A+\nu_0^A$		745	756
ν_{28}^X	869		798
ν_{27}^X	887		886
ν_{26}^X	957		930
(ν_{24}^X and $\nu_{28}^A+\nu_0^A$)[c]	1068	1140	1050
ν_{23}^X	1078		1071
ν_{22}^X	1110		1117
ν_{21}^X	1192		1135
$\nu_{27}^A+\nu_0^A$		1158	1155
$\nu_{26}^A+\nu_0^A$		1228	1201
ν_{20}^X	1256		1244
(ν_{19}^X and $\nu_{24}^A+\nu_0^A$)[c]	1307	1339	1300
ν_{18}^X	1338		1338
$\nu_{23}^A+\nu_0^A$		1349	1342
$\nu_{22}^A+\nu_0^A$		1381	1380
$\nu_{21}^A+\nu_0^A$		1463	1397
$\nu_{20}^A+\nu_0^A$		1527	1511
$\nu_{19}^A+\nu_0^A$		1578	1567
$\nu_{18}^A+\nu_0^A$		1609	1610

[a]See footnote a of Table VIII.

[b]Experimentally observed vibrational bands (in cm^{-1}) relative to the vibrationless level of the $\tilde{X}$ state ν_0^X.

[c]The experimental bands may have dual assignments.

(ν_{32}^X) cm^{-1} involves large CCO motion, 374 (ν_{31}^X) cm^{-1} is characterized by medium-sized CCO motion, 510 (ν_{30}^X) cm^{-1} includes large contribution from the CCO internal coordinate, 850 (ν_{28}^X) cm^{-1} contains a small-sized CO stretch character, 879 (ν_{27}^X) cm^{-1} is described by small CCO and small CO participation, 946 (ν_{26}^X) cm^{-1} may be attributed to medium CCO and medium CO participation, 1033 (ν_{25}^X) cm^{-1} involves a small CO stretch activity in its motion, 1061 (ν_{24}^X) cm^{-1} includes the internal coordinate of a medium character CO stretch motion, 1132 (ν_{22}^X) cm^{-1} refers to a medium character CCO deformation, 1285 (ν_{20}^X) cm^{-1} and 1329 (ν_{18}^X) cm^{-1} correspond to a small contribution of the CCO deformation internal coordinate in their modes, and 1362 (ν_{17}^X) cm^{-1} includes a small CO stretch character in its motion.

In the T_1T_2 conformation the $\tilde{A}$ state origin band appears relatively strong while it is somewhat diminished in the G_1T_2 conformer. In this sense the conformers of 1-butoxy show the same trend with respect to $\tilde{B}$-$\tilde{A}$ origin intensity as was suggested above for 1-propoxy. However, in G_1T_2 1-butoxy there is an observable band at 129 cm^{-1} which is likely the $\tilde{A}$ state origin. It then follows that there is a CO stretch progression in the $\tilde{A}$ state starting with the 1-0 line at 1196 cm^{-1} which we again associate with the mode ν_{23}^A. By comparison with the $\tilde{X}$ state assignments and having identified the $\tilde{A}$ state origin in the T_1G_2 conformer, it is a straightforward task to complete our assignments in the $\tilde{A}$ state. Other observed peaks are assigned in Table XII.

3. 2-Propoxy

The DF spectra for the unique conformer of 2-propoxy were recorded via two bands (*A* and *B* in Fig. 3), namely the origin band and the first member of the CO stretch progression. Figure 8 includes, in the top trace, the extended DF spectrum recorded via the first member of the CO progression in the $\tilde{B}$ state, and in the bottom trace an expanded view of the region redshifted up to $\approx$1300 cm^{-1} from the pumping frequency. The DF spectrum through the origin is almost identical with the spectrum recorded by pumping one quantum of CO stretch excitation but the latter has better signal/noise and we focus our analysis on it.

Our assignments for the nominally C_s 2-propoxy are necessarily built upon the same principles as for the primary alkoxies. For the $\tilde{X}$ state, we have identified a vibrational progression starting at 932 cm^{-1} redshifted from the pump-

TABLE XII. Assignment of the DF spectrum of the G_1T_2 conformer of 1-butoxy radical. The vibrational assignment is made for the emission pumping bands shown in Fig. 7.

Assignment	Frequency		
	Predicted[a]		Experimental[b]
	$\tilde{X}$	$\tilde{A}$	
ν_0^X			0
ν_0^A			129
ν_{33}^X	253		259
ν_{32}^X	341		337
ν_{31}^X	426		374
$\nu_{33}^A+\nu_0^A$		382	387
$\nu_{32}^A+\nu_0^A$		470	466
(ν_{30}^X and $\nu_{31}^A+\nu_0^A$)[c]	559	555	510
$\nu_{30}^A+\nu_0^A$		688	640
ν_{28}^X	855		850
ν_{27}^X	873		879
ν_{26}^X	960		946
$\nu_{28}^A+\nu_0^A$		984	979
$\nu_{27}^A+\nu_0^A$		1002	1008
ν_{25}^X	1030		1033
ν_{24}^X	1050		1061
(ν_{23}^X and $\nu_{26}^A+\nu_0^A$)[c]	1089	1089	1067
ν_{22}^X	1135		1132
$\nu_{25}^A+\nu_0^A$		1159	1162
$\nu_{24}^A+\nu_0^A$		1179	1190
$\nu_{23}^A+\nu_0^A$		1218	1196
$\nu_{22}^A+\nu_0^A$		1264	1260
ν_{20}^X	1271		1285
ν_{18}^X	1337		1329
ν_{17}^X	1370		1362
$\nu_{20}^A+\nu_0^A$		1400	1414
$\nu_{18}^A+\nu_0^A$		1466	1460
$\nu_{17}^A+\nu_0^A$		1499	1491

[a]See footnote a of Table VIII.

[b]Experimentally observed vibrational bands (in cm^{-1}) relative to the vibrationless level of the $\tilde{X}$ state ν_0^X.

[c]The experimental bands may have dual assignments.

ing frequency (see Fig. 8) with ν_{19}, a mode that bears significant CO stretch character (see Table VI). However, as Table VI shows in 2-propoxy, unlike the primary alkoxy radicals, there is a second mode ν_{14}, which has comparable CO stretch character. Referring to Table XIII we see that ν_{14} is assigned to a band at 1169 cm^{-1}. Clearly the 932 and 1169 cm^{-1} frequencies are much lower and higher, respectively, than the CO stretch frequencies deduced above for the primary alkoxies. We propose that when discussing CO stretch motion in 2-propoxy, and comparing it with other alkoxies, the average value, 1050 cm^{-1}, of these two frequencies be considered. Based upon the match (see Table XIII) with the calculated frequencies, we have assigned the other bands shown in the spectrum $\lesssim$1200 cm^{-1} to the vibrational modes placed within the parentheses (in cm^{-1}): 254 (ν_{26}^X), 398 (ν_{24}^X), 483 (ν_{23}^X), 837 (ν_{22}^X), 1002 (ν_{18}^X), 1033 (ν_{17}^X), and 1125 (ν_{15}^X). The character of each of the assigned modes in terms of its constituent internal coordinates is shown in Table VI.

The assignment of the $\tilde{A}$ state origin is somewhat challenging. After the above fairly straightforward $\tilde{X}$ state assignments, there are two relatively strong bands, in the low-frequency region at 68 and 524 cm^{-1}, which are plausible candidates. We favor the assignment of the $\tilde{B}$-$\tilde{X}$ origin to the

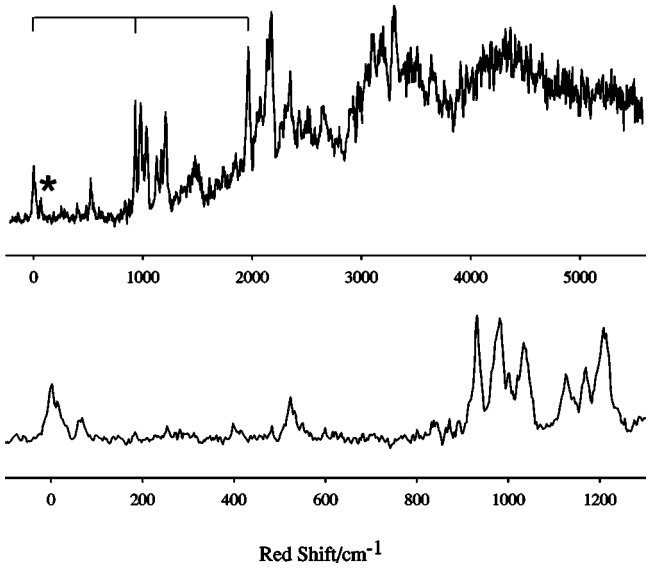

FIG. 8. DF spectra of 2-propoxy radical. The top trace was obtained by pumping band *B* (Fig. 3), the frequency of the first member of the CO stretch progression, at 27 734 cm^{-1}. The bottom trace corresponds to an expanded view of the DF data shown in the top trace. The *x* axis indicates (red) shift from the pump frequency. Assigned members of the predominant CO stretch progression ν_{19} are indicated by ticks on the top horizontal bar while the* indicates the line assigned to the $\tilde{A}$-$\tilde{X}$ origin transition. The intensities are not corrected for the grating efficiency and the camera sensitivity curves. The experimental resolution was 30–35 cm^{-1}.

TABLE XIII. Assignment of the DF spectrum pumped via the first member of the CO stretch progression of the excitation spectrum of 2-propoxy radical. The vibrational assignment is made for the emission pumping bands shown in Fig. 8.

Assignment	Frequency		
	Predicted[a]		Experimental[b]
	$\tilde{X}$	$\tilde{A}$	
ν_0^X			0
ν_0^A			68
ν_{26}^X	244		254
ν_{24}^X	390		398
ν_{23}^X	453		483
$\nu_{23}^A+\nu_0^A$		521	524
ν_{22}^X	809		837
$\nu_{22}^A+\nu_0^A$		877	892
ν_{19}^X	984		932
$\nu_{19}^A+\nu_0^A$		1052	981
ν_{18}^X	1054		1002
ν_{17}^X	1069		1033
$\nu_{18}^A+\nu_0^A$		1122	1054
ν_{15}^X	1207		1125
ν_{14}^X	1261		1169
($\nu_{14}^A+\nu_0^A$ and $\nu_{15}^A+\nu_0^A$)[c]		1329 and 1275	1208

[a]See footnote a of Table VIII.

[b]Experimentally observed vibrational bands (in cm^{-1}) relative to the vibrationless level of the $\tilde{X}$ state ν_0^X.

[c]The experimental bands may have dual assignments.

68 cm^{-1} band for a couple of reasons. First there seems no other explanation for a band at such a low frequency, as Table VI indicates the lowest vibrational frequency should be $\approx$200 cm^{-1}. In addition as Table III shows, both the calculated and experimental trends for the $\tilde{A}$-$\tilde{X}$ separation would indicate a value of $\lesssim$150 cm^{-1}, clearly inconsistent with an assignment to the 524 cm^{-1}. As Table XIII indicates there is a good frequency match for the 524 cm^{-1} band to $\nu_0^A+\nu_{23}^A$ assuming the ν_0^A assignment of 68 cm^{-1}. The main problem with the assignment is that there seems no particularly good reason for the relatively strong appearance of this band, although a very small $\tilde{A}$-$\tilde{X}$ separation may facilitate significant vibronic perturbations between the $\tilde{A}$ and $\tilde{X}$ states with resulting intensity anomalies. Using 68 cm^{-1} as the value for ν_0^A, the vibrational interval of the CO stretch progression formed in the $\tilde{A}$ state (attributed to ν_{19}^A) is, for the DF spectrum pumped via the origin of the $\tilde{B}$-$\tilde{X}$ LIF excitation, 904 cm^{-1} and for the spectrum pumped through its first CO stretch member 913 cm^{-1}, making an average of 908 cm^{-1}. Having the assignments to the $\tilde{X}$ state as a guide, we make corresponding assignments to the $\tilde{A}$ state as follows (in cm^{-1}): 892 (ν_{22}^A), 981 (ν_{19}^A), 1054 (ν_{18}^A), and 1208 (ν_{14}^A and ν_{15}^A unresolved).

4. 2-Butoxy

There are some important differences between the 2-butoxy spectra and the other species that we have observed. Like most of the other species there are multiple conformers, denoted $G+$, $G-$, and T (see Fig. 1) for a total of 3. However, unlike the other species there are no rotational analyses that assign a group of lines in the LIF spectrum to a given conformer. However, Fig. 10 shows that the DF spectra from lines *A* and *C* and separately *B* and *D* are nearly identical. Thus we believe that the LIF lines *A* and *C* likely belong to a given conformer, which we call *A*, and lines *B* and *D* belong to a second conformer, which we call *B*.

In addition to the conformer assignment issue, the general appearance of the 2-butoxy DF spectra is significantly different from the other species. Clearly there are fewer individual lines observed in the low-frequency, redshift region and as the frequency increases, the lines become broader and congestion becomes greater. There is also a tendency, as we will see below, not to see a precise repetition of fundamental frequencies in the combinations, nor a precise repetition between the $\tilde{A}$-$\tilde{X}$ intervals. We believe all of these effects stem from two factors: (i) the increasing size of the molecule with additional vibrational degrees of freedom and (ii) a small $\tilde{A}$-$\tilde{X}$ separation which combined with (i) engenders extensive vibronic interactions between the $\tilde{A}$ and $\tilde{X}$ states.

As a consequence of the above we limit ourselves to a somewhat less quantitative and less extensive analysis for 2-butoxy. Nonetheless, some quantitative information can be obtained from the spectra and is summarized in Tables XIV and XV. Using these Tables and Figs. 9 and 10 as a guide we can make the following observations. For conformer *A* there is a band at 125 cm^{-1}, much like the 68 cm^{-1} band in 2-propoxy. There is only one vibrational mode (see Tables 10–12 of the Supplementary Material), a backbone flex for which little intensity would be expected in the DF spectrum, at anywhere near this low a frequency. Hence like 2-propoxy, we assign this band to the $\tilde{B}$-$\tilde{A}$ origin. Turning to conformer *B*, a corresponding band appears at 55 cm^{-1}, which can be identified as the $\tilde{B}$-$\tilde{A}$ origin with even greater confidence.

As one would expect for both conformers there is a rela-

TABLE XIV. Assignment of the DF spectrum of the "*B*" conformer of 2-butoxy radical. The vibrational assignment is made for the emission pumping bands shown in Fig. 10.

Assignment	Frequency				
	Experimental[a](B)	Experimental[a](D)	Average[b]	Predicted[c]	
				$\tilde{X}$	$\tilde{A}$
ν_0^X	0	0	0		
ν_0^A	58	53	55		
$\nu_{30}^A+\nu_0^A$	509	509	509	529	
ν_{25}^X	929	929	929	989	
$\nu_{25}^A+\nu_0^A$	992	993	992		1044
ν_{23}^X	1045	1044	1044	1046	
$\nu_{23}^A+\nu_0^A$	1105	1104	1104		1101
ν_{20}^X	1142	1142	1142	1203	
$\nu_{20}^A+\nu_0^A$	1188	1187	1187		1258

[a]Experimentally observed vibrational bands (in cm^{-1}) relative to the excitation frequency of the vibrationless level of the $\tilde{X}$ state ν_0^X.
[b]The average values between the observed vibrational bands shown under the second and third column of the experimental results.
[c]Unscaled frequencies computed at the B3LYP/6-31+G* level of theory (in cm^{-1}). The vibrational levels of the $\tilde{A}$ state were estimated by adding the average of the two experimentally observed vibrationless levels of the $\tilde{A}$ state (denoted as ν_0^A) to the corresponding theoretically predicted frequencies under the column of assignment. The predicted frequencies were obtained for the *T* conformer which possibly correlates with bands *B* and *D*. See text for details. The assignment was made on the grounds that the PES for the lowest two energy states does not change considerably.

tively long CO stretch progression but only the first member of it has significantly resolved structure. In conformer *A*, it appears that there are four discernible lines (see Table XV) which we assign to the two bands with strongest CO stretch character for each the $\tilde{A}$ and $\tilde{X}$ states. Referring to Table XV we note the $\tilde{A}$-$\tilde{X}$ separations do not match those of the origin region all that well, but we attribute this to the strong vibronic interactions among the multiple levels in this region. For conformer *B*, the pattern is even more complex in the CO stretch region, but it is again at least consistent with that expected.

To this point, except for the $\tilde{A}$ state origin band, we have ignored the region redshifted $0-900\ cm^{-1}$. As the figures and tables show there is little activity in this region in our 2-butoxy spectra. Nonetheless there is one band around $500\ cm^{-1}$ ($554\ cm^{-1}$ in conformer *A* and $509\ cm^{-1}$ in conformer *B*). These are somewhat similar to a corresponding trend in this region for 2-propoxy, which we suggested was a possible, but not particularly likely, $\tilde{B}$-$\tilde{A}$ origin. The same must be said for the above bands in 2-butoxy. However, we feel the most likely assignment of this band is to ν_{31}^A for the *A* conformer and ν_{30}^A for the *B* conformer, although like 2-propoxy the reason for the relatively strong intensity for a band in this region is not obvious.

Before closing this section it is worth speculating a moment upon the correlation between the conformer labels *A* and *B* assigned to various spectral bands and the actual conformers, *G*+, *G*−, and *T* which have been the subject of

TABLE XV. Assignment of the DF spectrum of the "*A*" conformer of 2-butoxy radical. The vibrational assignment is made for the emission pumping bands shown in Fig. 10.

Assignment	Frequency				
	Experimental[a](A)	Experimental[a](C)	Average[b]	Predicted[c]	
				$\tilde{X}$	$\tilde{A}$
ν_0^X	0	0	0		
ν_0^A	129	121	125		
$\nu_{32}^A+\nu_0^A$	484	493	488		490
$\nu_{31}^A+\nu_0^A$	555	553	554		556
ν_{26}^X	916	916	916	936	
(ν_{24}^X and $\nu_{26}^A+\nu_0^A$)[d]	1000	1000	1000	1030	1061
(ν_{20}^X and $\nu_{24}^A+\nu_0^A$)[d]	1136	1134	1135	1194	1155
$\nu_{20}^A+\nu_0^A$	1253	1252	1252		1319

[a]Experimentally observed vibrational bands (in cm^{-1}) relative to the vibrationless level of the $\tilde{X}$ state ν_0^X.
[b]The average values between the observed vibrational bands shown under the second and third column of the experimental results.
[c]See footnote c of Table XIV. The predicted frequencies were obtained for the *G*+ conformer which possibly correlates with bands *A* and *C*. See text for details.
[d]The experimental bands may have multiple assignments.

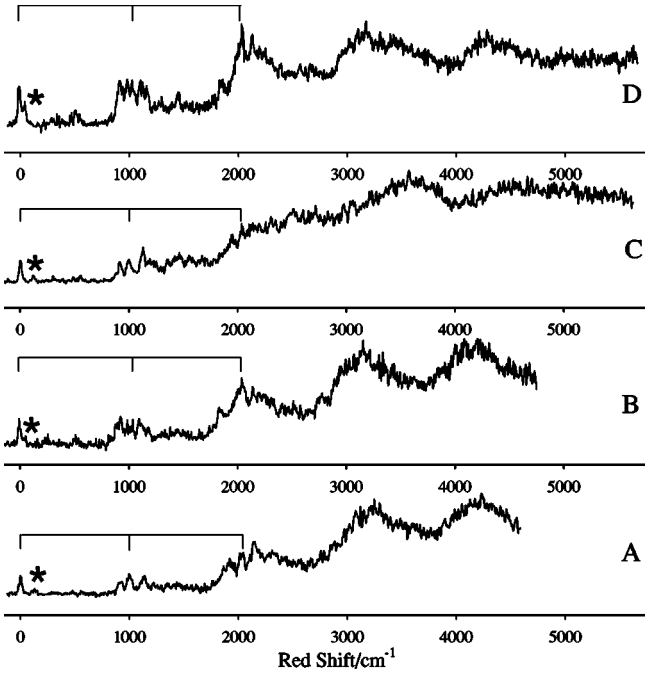

FIG. 9. DF spectra of the *A* and *B* conformations of 2-butoxy radical. The lowest trace was obtained by pumping band *A* (Fig. 3), the origin of the *A* conformer at 26 760 cm^{-1} while the next to the lowest trace was obtained by pumping band *B* (Fig. 3), the origin of the *B* conformer, at 27 068 cm^{-1}. The trace obtained by pumping band *C*, at 27 321 cm^{-1}, correspond to the transition to the first quantum of the CO stretch vibration of the *A* conformer in the $\tilde{B}$ state, while the trace through *D*, at 27 682 cm^{-1}, to the same type of excitation but for the *B* conformer. The *x* axis indicates (red) shift from the pump frequency. Assigned members of the predominant CO stretch progression, ν_{23} (conformer *B*) and ν_{24} (conformer *A*), are indicated by ticks on the top horizontal bar while the * indicates the line assigned to the $\tilde{A}$-$\tilde{X}$ origin transition. The intensities are not corrected for the grating efficiency and the camera sensitivity curves. The experimental resolution was 30–35 cm^{-1}.

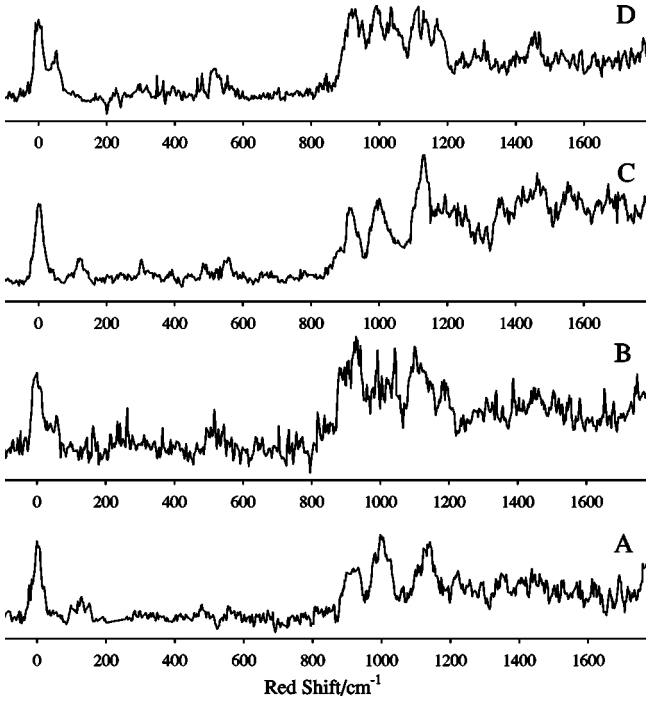

FIG. 10. An expanded view of the DF spectra of the *A* and *B* conformations of 2-butoxy radical. The lowest trace was obtained by pumping band *A* (Fig. 3), the origin of the *A* conformer at 26 760 cm^{-1} while the next to the lowest trace was obtained by pumping band *B* (Fig. 3), the origin of the *B* conformer, at 27 068 cm^{-1}. The trace obtained by pumping band *C*, at 27 321 cm^{-1}, corresponds to the transition to the first quantum of the CO stretch vibration of the *A* conformer in the $\tilde{B}$ state, while the trace through *D*, at 27682 cm^{-1}, to the same type of excitation but for the *B* conformer. The *x* axis indicates (red) shift from the pump frequency. The intensities are not corrected for the grating efficiency and the camera sensitivity curves. The experimental resolution was 30–35 cm^{-1}.

our quantum chemistry calculations. The proper way of making this correlation will be via the rotational analyses. However, the present studies at least provide some hints as to what the correlation may be.

It is useful to compare the C_1 symmetry 2-butoxy to 2-propoxy which has C_s symmetry. As we have previously observed the ''local'' symmetry around the O chromophore is the most important thing for determining the electronic structure and spectrum. Referring to Fig. 1, it is reasonable to argue that the local symmetry of *T* 2-butoxy is rather similar to 2-propoxy with *G*+ and *G*−, while having similar structures among themselves, are both somewhat distinguished from the *T* conformer. The qualitative observation is supported by the calculated vibrational frequencies of the three conformers in Tables 10–12 of the Supplementary Material. While the vibrational frequencies of all three conformers are collectively rather similar, some distinctions appear. For example all three conformers have two modes sharing the CO stretch character, but the lower frequency ones are almost identical (933 and 936 cm^{-1}) for the *G*− and *G*+ conformer while it is 989 cm^{-1} for the *T* conformer.

We note that there appear to be noticeable differences between the spectra of the *A* and *B* conformers. Based upon the above we expect one to be the *T* conformer while the other is either the *G*+ or *G*− conformer, with the *G*+ conformer more likely since it is computed to be the lowest energy and for the primary alkoxies the lowest energy conformer has always been observed.

If one accepts the above reasoning, it remains to suggest how *A* and *B* correlate to *G*+ and *T*. We argued earlier that the *T* conformer seems structurally more similar in the local O environment to 2-propoxy. Hence it may follow that the 55 cm^{-1} $\tilde{A}$-$\tilde{X}$ separation of the *B* conformer, being very similar to the 68 cm^{-1} value for 2-propoxy, makes it more likely correlated to the *T* conformer structure, leaving the *A* band for the *G*+ conformer. While we believe the analysis to be reasonable, we stress that definitive correlation must await relational analyses of the *A* and *B* conformer bands.

IV. DISCUSSION

There are two primary kinds of quantitative information that result from our DF studies of the alkoxy radicals, namely, the $\tilde{A}$-$\tilde{X}$ separations and the vibrational frequencies of the two states. We discuss these in turn and wrap up this section with some observations on qualitative aspects of the DF spectra.

It is important first to comment on the reliability of the $\tilde{A}$-$\tilde{X}$ separations from the DF data. The precision of these values is $\lesssim$10 cm^{-1} but given the inherent spectral complex-

ity there is always the possibility of assignment error. For example we now report a value of the $\tilde{A}$-$\tilde{X}$ separation for ethoxy although none was reported by Zhu, Kamal, and Misra[8] in their analysis of the DF spectrum. We have reassigned to the $\tilde{B}$-$\tilde{A}$ origin the line assigned by them to the fundamental vibration ν_{18} of the $\tilde{X}$ state. We believe that this is very reasonable given the fact that this vibrational frequency agreed least well of any they reported, when compared to those of similar molecules. It also is a relatively strong transition, consistent with the $\tilde{B}$-$\tilde{X}$ origin, but does not show a progression as expected for a strong vibrational band. Finally it is in good agreement with a value from a photoelectron detachment study[19] and qualitatively with quantum chemistry calculations.[12]

On the other hand, for 2-propoxy, the only other of these alkoxy radicals studied by electron detachment,[19] there is a marked discrepancy. However, if our value is correct, then it is fairly easy to understand an error in the electron detachment work. It is unlikely that an $\tilde{A}$-$\tilde{X}$ separation of 68 cm^{-1} would have been resolved in those studies. Therefore, an average $\approx$1225 cm^{-1} of two strong peaks was previously assigned as the $\tilde{A}$ state origin. We believe that transition corresponds to the CO stretch fundamental. In the report on the photodetachment work, the authors pointed out that their $\tilde{A}$ state assignment in 2-propoxy did not have the support of polarization data as did their assignment for ethoxy. We have pointed out the possibility of assigning our observed line at 524 cm^{-1} to the $\tilde{B}$-$\tilde{A}$ origin, but if the $\tilde{A}$-$\tilde{X}$ separation were this large it would be hard to understand while it was not observed in the photodetachment studies and it would be rather inconsistent with the quantum chemistry calculations, which as noted earlier are admittedly not very accurate for the $\tilde{A}$-$\tilde{X}$ separation. Finally we pointed out that for 2-butoxy again it is possible to assign a transition, giving a much larger $\tilde{A}$-$\tilde{X}$ separation ($\gtrsim$500 cm^{-1}) but the proponderance of the evidence favors the $\lesssim$130 cm^{-1} values.

With these comments we now turn to the discussion of the values of the $\tilde{A}$-$\tilde{X}$ separation in Table III. Several trends are apparent. For a given species the conformer with the C_s plane always has the largest $\tilde{A}$-$\tilde{X}$ separation and it appears the stronger the deviation from symmetry near the O atom chromophore, the more pronounced the decrease in splitting. For a given 1-alkoxy conformer, T_1 or G_1 near the oxygen atom, increasing the alkyl chain decreases the $\tilde{A}$-$\tilde{X}$ separation. Finally in going from a primary to a secondary alkoxy radical isomer, the $\tilde{A}$-$\tilde{X}$ separation decreases significantly.

These experimental results are quite valuable, since the energy of the excited $\tilde{A}$ state is quite important with respect to its participation in thermal reaction chemistry. Moreover, as we discussed earlier, the most advanced quantum chemistry calculations today can only give a qualitative idea at best as to its value.

The ability of calculations to predict vibrational frequencies is of course much better and we have strongly relied upon them for our vibrational assignments. However experiment clearly provides the "gold standard" for the frequencies as well. As we have shown the DF experiments measure a fairly large number of $\tilde{X}$ (and $\tilde{A}$) state vibrational frequencies for the alkoxies. Since modes involving the CO stretch character are the strongest we have the most information for them.

Table XVI summarizes the experimentally determined $\tilde{X}$ and $\tilde{A}$ state CO stretching frequencies of the alkoxy radicals investigated thus far. It also includes the $\tilde{B}$ state CO frequencies. It can immediately be noticed that the CO stretching frequency of the $\tilde{X}$ state is always larger than that of the $\tilde{B}$ state. The lowering of the frequency upon excitation is due to the expansion of the CO bond upon the electronic transition, as a consequence of exciting a bonding σ electron to a nonbonding, orbital localized on the O atom. Comparing the CO frequencies between the $\tilde{X}$ and $\tilde{A}$ states we notice an obvious similarity, a fact that is not surprising owing to the theoretically predicted similarity of the corresponding PESs.

The $\tilde{X}$ state CO stretch frequencies of the T conformer of 1-propoxy, and T_1T_2 and T_1G_2 conformations of 1-butoxy are almost identical and very similar to methoxy. The G conformer of 1-propoxy shows a similar CO frequency with the G_1T_2 conformer of 1-butoxy as well, but higher than the values for the other radicals. It seems that there is a consistent trend within the conformers of the primary alkoxies that involves a larger $\tilde{X}$ state CO stretching frequency for the conformers that have a G local electronic environment around oxygen.

We conclude our discussion with a few words about the general appearance of the DF spectra. As expected as the energy in the $\tilde{X}$ (or $\tilde{A}$) state increases the spectra become more congested and eventually discrete lines are not observed. It is also expected that this phenomenon occurs at progressively lower energy as the size of the radical increases.

However, what is not particularly expected is significantly different behavior for different isomers and conformers which is most clearly indicated for propoxy in Figs. 5 and 8. Striking is the degree of difference for the C_s conformers of 1- and 2-propoxy. Even more interesting is how different the spectra of the T and G conformers of 1-propoxy appear. Consider also the vast difference in the congestion in the T and G 1-propoxy spectra for the $\tilde{X}$ and $\tilde{A}$ states at nearly the same energy. These results indicate the vibronic coupling must be rather isomer and conformer specific with possible implications for internal vibrational redistribution and dynamics in these species. We are presently developing a picture of the coupling in the $\tilde{X}$, $\tilde{A}$, and $\tilde{B}$ states and plan to publish these results in the future.

V. CONCLUSION

DF spectra of the alkoxy radicals have been observed in a free jet expansion environment. Analysis of the spectra yields the energy separation between the vibrationless levels of the $\tilde{X}$ and $\tilde{A}$ states for most of the isomers and conformers of $C_nH_{2n+1}O$ for $n=3$ and 4. These studies also provide considerable insight into the $\tilde{X}$ and $\tilde{A}$ state vibrational structure. The CO stretch progression dominates for all DF spec-

TABLE XVI. Summary (in cm^{-1}) of experimentally determined $\tilde{X}$, $\tilde{A}$ and $\tilde{B}$ state vibrational fundamental frequencies of the CO stretch mode of the primary and secondary alkoxy radicals. The table summarizes the results of this work unless noted otherwise. The reported standard deviation of $\omega_e x_e$ is determined by the fit and it does not include the uncertainties of ω_0.

		$\tilde{X}$			$\tilde{A}$			$\tilde{B}$		
Alkoxies	Conformers	ω_0	ω_e	$\omega_e x_e$	ω_0	ω_e	$\omega_e x_e$	ω_0	ω_e	$\omega_e x_e$
Methoxy		1047(2)[a]	1057(3)[a]	7.0(7)[a]				662.4(5)[b]	667.4(1)[b]	2.56(3)[b]
ethoxy		1068 [c]	1078(2)[c]	6.2(4)[c]	991[c]			603[c]	609.4(3)[c]	2.96(5)[c]
1-propoxy	T	1050(10)	1055.8(5)	2.8(1)	1011(10)	1010.3(5)	−0.3(1)	676[d]		
	G	1066(10)	1072(3)	2.6(7)	1068(10)	1080(4)	3.9(8)	596[d]		
1-butoxy	T_1T_2	1052(10)	1055(1)	2.0(4)	1056(10)	1063(9)	6(2)	672[e]		
	T_1G_2	1051(10)	1058(2)	4.7(4)	1029(10)	1031(1)	0.4(2)			
	G_1T_2	1067(10)	1093(15)	10(4)	1067(10)	1092(16)	10(4)			
2-propoxy		1050(10)[f]			1026(10)[f]			569[g]	574.6(8)[g]	2.7(1)[g]
2-butoxy	B	1044(10)[h]			1049(10)[h]			611[i]		
	A	1000(10)[h]			1010(10)[h]			559[i]		

[a]Taken from Refs. 20 and 21.

[b]Data taken from Ref. 22. The least squares fit of the LIF data was done for $\nu=1-4$ of the CO stretch progression in the $\tilde{A}$ state. The first excited state of methoxy is designated as $\tilde{A}$, but owing to its electronically similar structure to the $\tilde{B}$ state of the rest of the reported alkoxy radicals, we report its spectroscopic characteristics under the column for the $\tilde{B}$ state.

[c]See Ref. 8. We have refitted the data of Table II for the CO stretch progressions in the $\tilde{X}$ and $\tilde{B}$ states and include the errors of ω_e and $\omega_e x_e$ in parenthesis. Based on our assignment of the $\tilde{A}$ state origin, we determined ω_0 of the CO stretch progression in the $\tilde{A}$ state.

[d]Taken from Ref. 5.

[e]Taken from Ref. 23.

[f]The frequency of 1050 cm^{-1} ($\tilde{X}$ state) is the average of 932 (ν_{19}^X) and 1169 (ν_{14}^X) cm^{-1}. The frequency of 1026 cm^{-1} ($\tilde{A}$ state) is the average of 913 (ν_{19}^A) and 1140 (ν_{14}^A) cm^{-1}. All of these values were determined from the DF spectrum that corresponds to emission from the $\nu=1$ CO stretch vibrational level of the $\tilde{B}$ state.

[g]Data taken from Ref. 3. The least squares fit of the LIF data was done for $\nu=1-6$ of the CO stretch progression in the $\tilde{B}$ state.

[h]The unresolved structure of the 2-butoxy DF spectra above 1500 cm^{-1} allowed only for the determination of the fundamental frequencies with any precision.

[i]Taken from Ref. 6.

tra providing the ν_{CO} stretching frequency for the $\tilde{X}$ state and in most cases for the $\tilde{A}$ state as well as numerous other vibrations. Quantum chemical calculations have been performed and compared with the experimental observations. Generally speaking, the experimental results agree well with the theoretical calculations. Observations are made concerning the degree of congestion of the DF spectra as the radical size increases.

ACKNOWLEDGMENTS

The authors gratefully acknowledge useful discussions with Lily Zu. The authors are pleased to acknowledge the support of parts of this research by the National Science Foundation via Grant No. 0211281, and other parts by the Chemical Sciences, Geosciences, and Biosciences Division, Office of Basic Energy Sciences, Office of Science, U.S. Department of Energy, via Grant No. DE-FG02-01ER15172. The authors also acknowledge a grant of computer time from the Ohio Supercomputer Center.

[1] M. E. Jenkin and G. D. Hayman, Atmos. Environ. **33**, 1275 (1999).
[2] R. Atkinson, Int. J. Chem. Kinet. **29**, 99 (1997).
[3] C. C. Carter, J. R. Atwell, S. Gopalakrishnan, and T. A. Miller, J. Phys. Chem. A **104**, 9165 (2000).
[4] C. C. Carter, S. Gopalakrishnan, J. R. Atwell, and T. A. Miller, J. Phys. Chem. A **105**, 2925 (2001).
[5] S. Gopalakrishnan, C. C. Carter, L. Zu, V. Stakhursky, G. Tarczay, and T. A. Miller, J. Chem. Phys. **118**, 4954 (2003).
[6] S. Gopalakrishnan, L. Zu, and T. A. Miller, J. Phys. Chem. A **107**, 5189 (2003).
[7] X. Liu, V. Stakhursky, E. D. Olmon, V. A. Lozovsky, T. A. Miller, and C. B. Moore, *58th OSU International Symposium on Molecular Spectroscopy* (The Ohio State University, Columbus, OH, 2003).
[8] X. Zhu, M. M. Kamal, and P. Misra, Pure Appl. Opt. **5**, 1021 (1996).
[9] A. H. Blatt, *Organic Synthesis, Collective Volume* (Wiley, New York, 1943).
[10] M. J. Frisch, G. W. Trucks, H. B. Schlegel *et al.*, GAUSSIAN 98, Revision A.7 (Gaussian, Inc., Pittsburgh, PA, 1998).
[11] J. F. Stanton, J. Gauss, W. J. Lauderdale, J. D. Watts, and R. J. Bartlett, The package also contains modified versions of the MOLECULE Gaussian integral program of J. Almlöf and P. R. Taylor, the ABACUS integral derivative program written by T. U. Helgaker, H. J. As. Jensen, P. Jørgensen, and P. R. Taylor, and the PROPS property evaluation integral code of P. R. Taylor.
[12] G. Tarczay, S. Gopalakrishnan, and T. A. Miller, J. Mol. Spectrosc. **220**, 276 (2003).
[13] See EPAPS Document No. E-JCPSA6-121-010446 for the calculated vibrational frequencies. A direct link to this document may be found in the online article's HTML reference section. The document may also be reached via the EPAPS homepage (http://www.aip.org/pubservs/epaps.html) or from ftp.aip.org in the directory /epaps/. See the EPAPS homepage for more information.
[14] R. S. Mulliken, J. Chem. Phys. **23**, 1997 (1953).
[15] A. G. Császár, W. D. Allen, Y. Yamaguchi, and H. F. Schaefer, in *Computational Molecular Spectroscopy*, edited by J. Jensen and P. R. Bunker (Wiley, New York, 2000), Chap. 2.
[16] E. R. Davidson and W. T. Borden, J. Phys. Chem. **87**, 4783 (1983).
[17] J. F. Stanton, Chem. Phys. Lett. **237**, 20 (1995).
[18] J. F. Stanton, J. Chem. Phys. **115**, 10382 (2001).
[19] T. M. Ramond, G. E. Davico, R. L. Schwartz, and W. C. Lineberger, J. Chem. Phys. **112**, 1158 (2000).
[20] Y.-Y. Lee, G.-H. Wann, and Y.-P. Lee, J. Chem. Phys. **99**, 9465 (1993).
[21] S. C. Foster, P. Misra, T.-Y. D. Lin, C. P. Damo, C. C. Carter, and T. A. Miller, J. Phys. Chem. **92**, 5914 (1988).
[22] D. E. Powers, M. B. Pushkarsky, and T. A. Miller, J. Chem. Phys. **106**, 6863 (1997).
[23] S. Gopalakrishnan, L. Zu, and T. A. Miller, Chem. Phys. Lett. **380**, 749 (2003).